

Reciprocity Calibration of Dual-Antenna Repeaters via MMSE Estimation

Shoma Hara, *Graduate Student Member, IEEE*, Takumi Takahashi, *Member, IEEE*, Hiroki Iimori, *Member, IEEE*, Hideki Ochiai, *Fellow, IEEE*, Erik G. Larsson, *Fellow, IEEE*

Abstract—This paper proposes a novel Bayesian reciprocity calibration method that consistently ensures uplink and downlink channel reciprocity in repeater-assisted multiple-input multiple-output (MIMO) systems. The proposed algorithm is formulated under the minimum mean-square error (MMSE) criterion. Its Bayesian framework incorporates complete statistical knowledge of the signal model, noise, and prior distributions, enabling a coherent design that achieves both low computational complexity and high calibration accuracy. To further enhance phase-alignment accuracy, which is critical for calibration tasks, we develop a von Mises denoiser that exploits the fact that the target parameters lie on the circle in the complex plane. Simulation results demonstrate that the proposed MMSE algorithm achieves substantially improved estimation accuracy compared with conventional deterministic non-linear least-squares (NLS) methods, while maintaining comparable computational complexity. Furthermore, the proposed method exhibits remarkably fast convergence, making it well suited for practical implementation.

Index Terms—Reciprocity calibration, dual-antenna repeater, MIMO systems, Bayesian inference, MMSE

I. INTRODUCTION

Massive multiple-input multiple-output (MIMO) systems rely on time-division duplexing (TDD) channel reciprocity to enable scalable channel state information (CSI) acquisition at the base station (BS) [1], [2]. In TDD operation, the BS estimates uplink channels from pilot transmissions and reuses them for downlink precoding, leveraging the large antenna array to coherently combine low-power uplink signals. However, while reciprocity holds for the physical propagation channel, practical transceiver hardware exhibits non-reciprocal behavior due to mismatches between the transmit (TX) and receive (RX) radio frequency (RF) chains [3], which distort the effective uplink and downlink channels observed at the BS. As a result, uplink-based channel estimates cannot be directly reused for downlink precoding without compensation, making reciprocity calibration a fundamental requirement for accurate beamforming and for realizing the full performance potential of reciprocity-based massive MIMO systems [4].

The problem of reciprocity calibration in TDD-based MIMO systems was formally identified and formulated in

S. Hara, T. Takahashi and H. Ochiai are with the Graduate School of Engineering, University of Osaka, 2-1 Yamada-oka, Suita, 565-0871, Japan (e-mail: s-hara@wcs.comm.eng.osaka-u.ac.jp, {takahashi, ochiai}@comm.eng.osaka-u.ac.jp). H. Iimori is with Ericsson Research, Ericsson Japan K. K., Yokohama SYMPHOSTAGE West Tower 12F, 5-1-2 Minato Mirai, Yokohama, 220-0012, Japan (e-mail: hiroki.iimori@ericsson.com). E. G. Larsson is with the Department of Electrical Engineering (ISY), Linköping University, 581 83 Linköping, Sweden (e-mail: erik.g.larsson@liu.se).

A conference version of this work is planned to be submitted to a special session at IEEE SPAWC 2026. This work has been submitted to the IEEE for possible publication. Copyright may be transferred without notice, after which this version may no longer be accessible.

early work [5]. This line of research established a fundamental calibration model in which the observed uplink and downlink channels differ by multiplicative hardware responses and demonstrated that accurate downlink beamforming requires explicit compensation of these non-reciprocal effects. Following this formulation, extensive research has developed reciprocity calibration methods for conventional massive MIMO systems with co-located antenna arrays. Representative approaches include relative calibration techniques that exploit internal signal exchange or mutual coupling among antennas within the same array [6], as well as over-the-air schemes based on bidirectional pilot transmissions [7]. Under the assumption of a single-hop channel and co-located hardware, these methods can estimate the relative TX and RX responses of the BS antenna elements up to a common scalar ambiguity, which is sufficient for multiuser downlink precoding since this scalar does not affect beamforming directions or interference suppression.

Recent cellular network architectures are evolving beyond conventional co-located BSs toward more spatially distributed deployments to improve coverage, spatial multiplexing capability, and user experience at the cell edge [8]–[12]. While distributed massive MIMO systems have been extensively studied to improve spatial diversity, coverage uniformity, and cell-edge performance by geographically separating antenna elements, their practical deployment remains challenging. Distributed MIMO architectures typically rely on high-capacity, low-latency fronthaul or backhaul connections to coordinate multiple remote radio units, which significantly increases deployment cost and operational complexity [13].

In light of these challenges, repeater-assisted massive MIMO has emerged as a pragmatic alternative that enables network densification without the architectural complexity of fully distributed deployments [14]–[23]. By deploying physically small and low-cost wireless repeaters within the cell, additional effective scattering paths are created, improving coverage and channel rank while keeping all multi-antenna signal processing centralized at the BS. Unlike distributed access points, repeaters do not require dedicated backhaul, tight inter-site synchronization, or major changes to existing network architectures, making them attractive from both deployment and maintenance perspectives. Ongoing standardization efforts on network-controlled repeaters further highlight their relevance as a realistic step toward performance levels approaching those of distributed massive MIMO systems [24].

Conventional reciprocity calibration methods are developed under the assumption that the channel between the BS and the user equipments (UEs) is a single-hop propagation channel, affected only by the TX and RX hardware chains at the transceiver endpoints. In repeater-assisted architectures, this

assumption no longer holds. Repeaters introduce additional TX and RX chains with their own analog impairments, amplification gains, and phase responses, which become cascaded with the BS-UE channel [25]. As a result, the effective end-to-end channel is composed not only of the propagation environment and the BS/UE hardware but also of unknown and potentially asymmetric forward and reverse responses of the repeater. This cascaded non-reciprocity fundamentally alters the structure of the calibration problem and renders standard massive MIMO calibration techniques designed for co-located arrays and direct links insufficient.

Only recently has repeater-induced non-reciprocity been addressed explicitly in the literature, although earlier works, *e.g.*, [26], had already suggested that repeaters may not operate effectively in TDD systems due to their inherently non-reciprocal behavior. To address this issue, a calibration method has recently been proposed in which the repeater-induced hardware asymmetries are explicitly modeled and incorporated into the reciprocity calibration problem through a coupled least-squares (LS) formulation [27]. The resulting estimation problem is solved using a non-linear least-squares (NLS) and alternating NLS approach to handle the coupling among multiple unknown hardware responses. While this formulation represents an important step toward repeater-aware reciprocity calibration, the proposed solution is developed within a deterministic LS framework and treats the repeater-induced hardware impairments as unknown but unstructured quantities. In practice, prior information on these impairments may be available. Leveraging such prior information has the potential to significantly improve calibration robustness and accuracy, especially under limited training overhead or low signal-to-noise ratio (SNR) conditions. This observation motivates the development of the proposed calibration algorithm in this paper. Our specific contributions are:

- We develop a Bayesian formulation of the repeater-aware reciprocity calibration problem by explicitly incorporating prior statistical models of the repeater-induced non-reciprocity and the measurement noise, enabling a principled treatment of hardware-induced impairments.
- Building upon this formulation, we propose a novel minimum mean-square error (MMSE)-based calibration algorithm that performs iterative Bayesian bilinear inference using probabilistic data association (PDA) [28]–[30], where the MMSE updates are implemented via von Mises denoisers and unknown prior statistics are estimated through the method of moments (MoM).
- Through extensive simulations, we demonstrate that the proposed algorithm achieves significantly improved robustness and accuracy over the state-of-the-art (SotA) deterministic NLS methods [27] in large-scale and low SNR regimes, while maintaining computational complexity comparable to the basic NLS method.

Notation: Sets of real and complex-valued numbers are denoted by \mathbb{R} and \mathbb{C} , respectively. Vectors and matrices are denoted by lowercase and uppercase letters, respectively. The (i, j) -th entry of a matrix \mathbf{A} is denoted by $\mathbf{A}(i, j)$, and the i -th column of \mathbf{A} is denoted by $(\mathbf{A})_i$. The $a \times a$ square identity matrix is denoted by \mathbf{I}_a . For scalars a_1, \dots, a_M , $\text{diag}(a_1, \dots, a_M)$ denotes a diagonal matrix with the elements

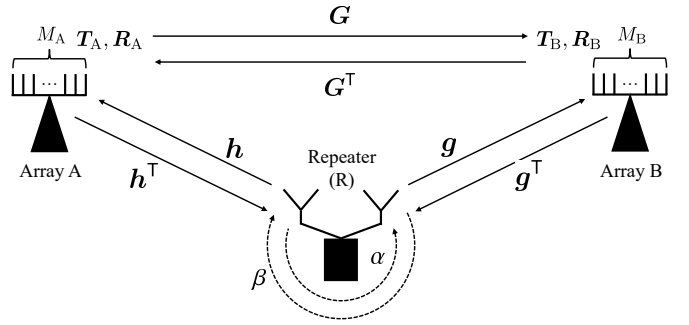


Fig. 1. Two antenna arrays, A and B, and a repeater (R). \mathbf{G} denotes the propagation channel from A to B when R is turned off. Radio channels are represented by solid lines, whereas repeater gains are represented by dashed lines. The figure is adapted from [27].

a_1, \dots, a_M on its main diagonal. The conjugate, transpose, and Hermitian transpose are denoted by $(\cdot)^*$, $(\cdot)^T$, and $(\cdot)^H$, respectively. The trace and determinant of \mathbf{A} are denoted by $\text{tr}(\mathbf{A})$ and $\det(\mathbf{A})$, respectively. The Kronecker product of matrices \mathbf{A} and \mathbf{B} is denoted by $\mathbf{A} \otimes \mathbf{B}$. The stacking of the columns of a matrix \mathbf{A} on top of one another is denoted by $\text{vec}(\mathbf{A})$. The symbol $\|\cdot\|_2$ and $\|\cdot\|_F$ denote the Euclidean norm of a vector and the Frobenius norm of a matrix, respectively. The real part of a complex quantity is denoted by $\Re\{\cdot\}$, and the imaginary unit is denoted by $j \triangleq \sqrt{-1}$. The magnitude and phase of a complex number c are denoted by $|c|$ and $\arg(c)$, respectively. The notation $a \sim \mathcal{P}$ indicates that a random variable a follows a probability distribution \mathcal{P} . The circularly symmetric complex Gaussian distribution with mean μ and covariance Λ is denoted by $\mathcal{CN}(\mu, \Lambda)$. The real Gaussian distribution with mean μ and variance σ^2 is denoted by $\mathcal{N}(\mu, \sigma^2)$. The uniform distribution on $[a, b]$ is denoted by $\mathcal{U}[a, b]$. The probability density function (PDF) of x is denoted by $p_x(\cdot)$, and the conditional PDF of x given y is denoted by $p_{x|y}(\cdot| \cdot)$. The expectation is denoted by $\mathbb{E}[\cdot]$. Finally, the notation $\mathcal{O}(\cdot)$ denotes the computational complexity order.

II. SYSTEM MODEL

Consider a communication scenario comprising two antenna arrays, denoted by A and B, and a dual-antenna repeater R, as illustrated in Fig. 1 [27]. The numbers of antennas at arrays A and B are denoted by M_A and M_B , respectively. In practice, A and B may represent a BS and a mobile user terminal, or two distributed access points in a distributed MIMO system.

The propagation channel between A and B consists of a direct path and an indirect path through the repeater R. When the repeater is switched off, the direct channel from A to B is denoted by $\mathbf{G} \in \mathbb{C}^{M_B \times M_A}$, and, by reciprocity, the channel from B to A is given by \mathbf{G}^T . We impose no structural assumptions on \mathbf{G} ; it may include both line-of-sight (LoS) and multipath components. Even when R is deactivated, it may scatter incident radio waves and thus serve as a reciprocal passive element, an effect implicitly captured in \mathbf{G} .

The channel from A to R is denoted by $\mathbf{h}^T \in \mathbb{C}^{1 \times M_A}$, and the reverse channel from R to A is denoted by $\mathbf{h} \in \mathbb{C}^{M_A \times 1}$. Similarly, the channel from B to R is represented by $\mathbf{g}^T \in \mathbb{C}^{1 \times M_B}$, and the reverse channel from R to B is denoted by $\mathbf{g} \in \mathbb{C}^{M_B \times 1}$. When the repeater operates in its nominal

configuration, the complex gains of the forward and reverse paths are denoted by α and β , respectively. In general, $\alpha \neq \beta$, implying that the repeater is nominally non-reciprocal. This non-reciprocity arises from factors such as thermal fluctuations and hardware non-idealities.

In addition, the TX and RX branches of arrays A and B introduce hardware-induced non-reciprocity due to analog front-end impairments such as temperature drift and long-term component aging. This non-reciprocity is modeled by four diagonal matrices,

$$\mathbf{T}_A \triangleq \text{diag}(t_{A,1}, t_{A,2}, \dots, t_{A,M_A}), \quad (1a)$$

$$\mathbf{R}_A \triangleq \text{diag}(r_{A,1}, r_{A,2}, \dots, r_{A,M_A}), \quad (1b)$$

$$\mathbf{T}_B \triangleq \text{diag}(t_{B,1}, t_{B,2}, \dots, t_{B,M_B}), \quad (1c)$$

$$\mathbf{R}_B \triangleq \text{diag}(r_{B,1}, r_{B,2}, \dots, r_{B,M_B}), \quad (1d)$$

whose diagonal entries represent the complex-valued reciprocity coefficients of the individual antenna elements, including a possible drift of the oscillators at A and B.

Using the above definitions, the effective noise-free channel from A to B can be expressed as

$$\mathbf{R}_B (\mathbf{G} + \alpha \mathbf{g} \mathbf{h}^\top) \mathbf{T}_A, \quad (2)$$

while the channel from B to A is given by

$$\mathbf{R}_A (\mathbf{G}^\top + \beta \mathbf{h} \mathbf{g}^\top) \mathbf{T}_B. \quad (3)$$

In each expression, the first term represents the direct propagation channel, whereas the second term captures the repeater-assisted path.

For generality, neither array A nor B is assumed to be pre-calibrated. Consequently, all parameters

$$\alpha, \beta, \mathbf{G}, \mathbf{g}, \mathbf{h}, \mathbf{R}_A, \mathbf{T}_A, \mathbf{R}_B, \mathbf{T}_B$$

are treated as *a priori* unknown.

III. STATE-OF-THE-ART CALIBRATION SCHEME

We now describe the SotA reciprocity calibration scheme for dual-antenna repeaters presented in [27]. The key idea is to estimate the ratio between the forward and reverse repeater gains, α and β , using bi-directional pilot transmissions between arrays A and B under two distinct repeater configurations. Specifically, two sets of measurements are conducted within one channel coherence interval:

- (i) bi-directional transmission with R operating in its nominal configuration, and
- (ii) bi-directional transmission with R configured to apply a π -phase shift to both the forward and reverse gains.

This procedure yields four channel measurements as follows:

$$\mathbf{X}_{AB}^0 = \mathbf{R}_B (\mathbf{G} + \alpha \mathbf{g} \mathbf{h}^\top) \mathbf{T}_A + \mathbf{W}_B^0, \quad (4a)$$

$$\mathbf{X}_{BA}^0 = \mathbf{R}_A (\mathbf{G}^\top + \beta \mathbf{h} \mathbf{g}^\top) \mathbf{T}_B + \mathbf{W}_A^0, \quad (4b)$$

$$\mathbf{X}_{AB}^1 = \mathbf{R}_B (\mathbf{G} - \alpha \mathbf{g} \mathbf{h}^\top) \mathbf{T}_A + \mathbf{W}_B^1, \quad (4c)$$

$$\mathbf{X}_{BA}^1 = \mathbf{R}_A (\mathbf{G}^\top - \beta \mathbf{h} \mathbf{g}^\top) \mathbf{T}_B + \mathbf{W}_A^1, \quad (4d)$$

where $\mathbf{W}_B^0 \in \mathbb{C}^{M_B \times M_A}$, $\mathbf{W}_A^0 \in \mathbb{C}^{M_A \times M_B}$, $\mathbf{W}_B^1 \in \mathbb{C}^{M_B \times M_A}$, and $\mathbf{W}_A^1 \in \mathbb{C}^{M_A \times M_B}$ denote the measurement noise matrices.

The objective of calibration is to determine the ratio

$$\gamma \triangleq \frac{\beta}{\alpha}, \quad (5)$$

since knowledge of γ allows the repeater to be configured such that $\alpha = \beta$, thereby rendering it reciprocal to the network.

To address this estimation, the model is re-parameterized as

$$\mathbf{H} \triangleq \mathbf{R}_B \mathbf{G} \mathbf{T}_A \in \mathbb{C}^{M_B \times M_A}, \quad (6a)$$

$$\mathbf{A} \triangleq \mathbf{T}_A^{-1} \mathbf{R}_A \in \mathbb{C}^{M_A \times M_A}, \quad (6b)$$

$$\mathbf{B} \triangleq \mathbf{T}_B \mathbf{R}_B^{-1} \in \mathbb{C}^{M_B \times M_B}, \quad (6c)$$

$$\mathbf{Z} \triangleq \alpha \mathbf{R}_B \mathbf{g} \mathbf{h}^\top \mathbf{T}_A \in \mathbb{C}^{M_B \times M_A}, \quad (6d)$$

which leads to the equivalent measurement equations:

$$\mathbf{X}_{AB}^0 = \mathbf{H} + \mathbf{Z} + \mathbf{W}_B^0, \quad (7a)$$

$$\mathbf{X}_{BA}^0 = \mathbf{A}(\mathbf{H} + \gamma \mathbf{Z})^\top \mathbf{B} + \mathbf{W}_A^0, \quad (7b)$$

$$\mathbf{X}_{AB}^1 = \mathbf{H} - \mathbf{Z} + \mathbf{W}_B^1, \quad (7c)$$

$$\mathbf{X}_{BA}^1 = \mathbf{A}(\mathbf{H} - \gamma \mathbf{Z})^\top \mathbf{B} + \mathbf{W}_A^1. \quad (7d)$$

After straightforward calculations, the preprocessed measurements for the calibration task are obtained as follows:

$$\mathbf{R}_1 \triangleq \frac{1}{2} (\mathbf{X}_{AB}^0 + \mathbf{X}_{AB}^1) = \mathbf{H} + \mathbf{W}_1, \quad (8a)$$

$$\mathbf{R}_2 \triangleq \frac{1}{2} (\mathbf{X}_{AB}^0 - \mathbf{X}_{AB}^1) = \mathbf{Z} + \mathbf{W}_2, \quad (8b)$$

$$\mathbf{R}_3 \triangleq \frac{1}{2} (\mathbf{X}_{BA}^0 + \mathbf{X}_{BA}^1) = \mathbf{A} \mathbf{H}^\top \mathbf{B} + \mathbf{W}_3, \quad (8c)$$

$$\mathbf{R}_4 \triangleq \frac{1}{2} (\mathbf{X}_{BA}^0 - \mathbf{X}_{BA}^1) = \gamma \mathbf{A} \mathbf{Z}^\top \mathbf{B} + \mathbf{W}_4, \quad (8d)$$

where

$$\mathbf{W}_1 \triangleq \frac{1}{2} (\mathbf{W}_B^0 + \mathbf{W}_B^1), \quad \mathbf{W}_2 \triangleq \frac{1}{2} (\mathbf{W}_B^0 - \mathbf{W}_B^1),$$

$$\mathbf{W}_3 \triangleq \frac{1}{2} (\mathbf{W}_A^0 + \mathbf{W}_A^1), \quad \mathbf{W}_4 \triangleq \frac{1}{2} (\mathbf{W}_A^0 - \mathbf{W}_A^1).$$

Based on (8), the parameters defined in (6) are jointly estimated by minimizing the following NLS criterion [27]

$$f = \|\mathbf{R}_1 - \mathbf{H}\|_F^2 + \|\mathbf{R}_2 - \mathbf{Z}\|_F^2 + \|\mathbf{R}_3 - \mathbf{A} \mathbf{H}^\top \mathbf{B}\|_F^2 + \|\mathbf{R}_4 - \gamma \mathbf{A} \mathbf{Z}^\top \mathbf{B}\|_F^2. \quad (9)$$

The resulting solution provides a statistically consistent estimate of γ , enabling reciprocity calibration of the repeater.

A. NLS Algorithm

Based on (9), the following stepwise algorithm is employed for practical parameter estimation.

- 1) *Estimation of \mathbf{H} :* From the averaged measurements in (8a), the minimizer with respect to (w.r.t.) \mathbf{H} is

$$\hat{\mathbf{H}} = \mathbf{R}_1. \quad (10)$$

- 2) *Estimation of \mathbf{Z} :* Using (8b), the estimate of \mathbf{Z} is obtained as

$$\hat{\mathbf{Z}} = \mathcal{S}\{\mathbf{R}_2\}, \quad (11)$$

where $\mathcal{S}\{\cdot\}$ denotes the best rank-one approximation of a matrix, obtained from its dominant singular vector pair.

- 3) *Estimation of \mathbf{A} and \mathbf{B} :* From (8c), the matrices \mathbf{A} and \mathbf{B} are estimated by alternating projections. Starting from the initial values $\hat{\mathbf{A}} = \mathbf{I}_{M_A}$ and $\hat{\mathbf{B}} = \mathbf{I}_{M_B}$, each diagonal element

Algorithm 1 : NLS-based calibration algorithm**Input:** $\mathbf{R}_1, \mathbf{R}_2, \mathbf{R}_3, \mathbf{R}_4$ **Output:** $\hat{\mathbf{H}}, \hat{\mathbf{Z}}, \hat{\mathbf{A}}, \hat{\mathbf{B}}, \hat{\gamma}$

```

// 1) Estimation of  $\mathbf{H}$ 
1:  $\hat{\mathbf{H}} \leftarrow \mathbf{R}_1$ 
// 2) Estimation of  $\mathbf{Z}$ 
2:  $\hat{\mathbf{Z}} \leftarrow \mathcal{S}\{\mathbf{R}_2\}$ 
// 3) Estimation of  $\mathbf{A}$  and  $\mathbf{B}$ 
3:  $\hat{\mathbf{A}} \leftarrow \mathbf{I}_{M_A}, \hat{\mathbf{B}} \leftarrow \mathbf{I}_{M_B}$  ▷ Initialization
4: repeat
5:  $\forall i \in \mathcal{A} : \hat{\mathbf{A}}(i, i) \leftarrow \frac{(\hat{\mathbf{B}}\hat{\mathbf{H}})_i^H(\mathbf{R}_3^T)_i}{\|(\hat{\mathbf{B}}\hat{\mathbf{H}})_i\|_2^2}$ 
6:  $\forall j \in \mathcal{B} : \hat{\mathbf{B}}(j, j) \leftarrow \frac{(\hat{\mathbf{A}}\hat{\mathbf{H}}^T)_j^H(\mathbf{R}_3)_j}{\|(\hat{\mathbf{A}}\hat{\mathbf{H}}^T)_j\|_2^2}$ 
7:  $\hat{\mathbf{A}} \leftarrow \hat{\mathbf{A}} \cdot \|\hat{\mathbf{B}}\|_F$ 
8:  $\hat{\mathbf{B}} \leftarrow \hat{\mathbf{B}} / \|\hat{\mathbf{B}}\|_F$ 
9: until Num. of iterations reaches  $N_{\text{Iter}}$ 
// 4) Estimation of  $\gamma$ 
10:  $\hat{\gamma} \leftarrow \frac{\text{tr}\{(\hat{\mathbf{A}}\hat{\mathbf{Z}}^T\hat{\mathbf{B}})^H\mathbf{R}_4\}}{\|\hat{\mathbf{A}}\hat{\mathbf{Z}}^T\hat{\mathbf{B}}\|_F^2}$ 

```

is iteratively updated as

$$\hat{\mathbf{A}}(i, i) = \frac{(\hat{\mathbf{B}}\hat{\mathbf{H}})_i^H(\mathbf{R}_3^T)_i}{\|(\hat{\mathbf{B}}\hat{\mathbf{H}})_i\|_2^2}, \forall i \in \mathcal{A}, \quad (12a)$$

$$\hat{\mathbf{B}}(j, j) = \frac{(\hat{\mathbf{A}}\hat{\mathbf{H}}^T)_j^H(\mathbf{R}_3)_j}{\|(\hat{\mathbf{A}}\hat{\mathbf{H}}^T)_j\|_2^2}, \forall j \in \mathcal{B}, \quad (12b)$$

where $\mathcal{A} \triangleq \{1, 2, \dots, M_A\}$ and $\mathcal{B} \triangleq \{1, 2, \dots, M_B\}$. Normalization is applied at each iteration to prevent numerical instability [27].

4) *Estimation of γ :* Using (8d),

$$\mathbf{R}_4 = \frac{1}{2} (\mathbf{X}_{\text{BA}}^0 - \mathbf{X}_{\text{BA}}^1), \quad (13)$$

the gain ratio is estimated as

$$\hat{\gamma} = \frac{\text{tr}\{(\hat{\mathbf{A}}\hat{\mathbf{Z}}^T\hat{\mathbf{B}})^H\mathbf{R}_4\}}{\|\hat{\mathbf{A}}\hat{\mathbf{Z}}^T\hat{\mathbf{B}}\|_F^2}. \quad (14)$$

This NLS algorithm yields an approximate solution to the original criterion given in (9). The procedure described above is summarized in Algorithm 1.

B. Alternating-Optimization NLS Algorithm

From (8), the information of \mathbf{H} is contained not only in \mathbf{R}_1 but also in \mathbf{R}_3 , and the information of \mathbf{Z} is contained not only in \mathbf{R}_2 but also in \mathbf{R}_4 . Therefore, further performance improvement can be achieved by performing alternating optimization over all unknown variables, *i.e.*, \mathbf{H} , \mathbf{Z} , \mathbf{A} , \mathbf{B} , and γ . For details, we refer the reader to [27], and for completeness, only the pseudocode is provided in Algorithm 2. However, this approach incurs a higher computational complexity.

IV. PROPOSED MMSE ALGORITHM

The SotA methods are designed based on the NLS criterion and therefore cannot exploit available statistical in-

Algorithm 2 : Alternating-opt. NLS-based algorithm**Input:** $\mathbf{R}_1, \mathbf{R}_2, \mathbf{R}_3, \mathbf{R}_4$ **Output:** $\hat{\mathbf{H}}, \hat{\mathbf{Z}}, \hat{\mathbf{A}}, \hat{\mathbf{B}}, \hat{\gamma}$

```

/* ----- Initialization ----- */
1: Obtain initial estimates  $\hat{\mathbf{H}}, \hat{\mathbf{Z}}, \hat{\mathbf{A}}, \hat{\mathbf{B}}, \hat{\gamma}$  using Alg. 1.
/* ----- Alternating optimization ----- */
2: repeat
    // 1) Update of  $\mathbf{H}$ 
    3:  $\mathbf{r} \leftarrow [\text{vec}(\mathbf{R}_1); \text{vec}(\mathbf{R}_3^T)], \boldsymbol{\Xi} \leftarrow [\mathbf{I}_{M_A} \otimes \mathbf{I}_{M_B}; \hat{\mathbf{A}} \otimes \hat{\mathbf{B}}]$ 
    4:  $\text{vec}(\hat{\mathbf{H}}) \leftarrow (\boldsymbol{\Xi}^H \boldsymbol{\Xi})^{-1} \boldsymbol{\Xi}^H \mathbf{r}$ 
        // 2) Update of  $\mathbf{A}$  and  $\mathbf{B}$ 
    5: repeat
        // 1) Update of  $\mathbf{Z}$ 
        6:  $\forall i \in \mathcal{A} : \hat{\mathbf{A}}(i, i) \leftarrow \frac{(\hat{\mathbf{B}}\hat{\mathbf{H}})_i^H(\mathbf{R}_3^T)_i + \hat{\gamma}^* (\hat{\mathbf{B}}\hat{\mathbf{Z}})_i^H(\mathbf{R}_4^T)_i}{\|(\hat{\mathbf{B}}\hat{\mathbf{H}})_i\|_2^2 + |\hat{\gamma}|^2 \|(\hat{\mathbf{B}}\hat{\mathbf{Z}})_i\|_2^2}$ 
        7:  $\forall j \in \mathcal{B} : \hat{\mathbf{B}}(j, j) \leftarrow \frac{(\hat{\mathbf{A}}\hat{\mathbf{H}}^T)_j^H(\mathbf{R}_3)_j + \hat{\gamma}^* (\hat{\mathbf{A}}\hat{\mathbf{Z}}^T)_j^H(\mathbf{R}_4)_j}{\|(\hat{\mathbf{A}}\hat{\mathbf{H}}^T)_j\|_2^2 + |\hat{\gamma}|^2 \|(\hat{\mathbf{A}}\hat{\mathbf{Z}}^T)_j\|_2^2}$ 
        8:  $\hat{\mathbf{A}} \leftarrow \hat{\mathbf{A}} \cdot \|\hat{\mathbf{B}}\|_F$ 
        9:  $\hat{\mathbf{B}} \leftarrow \hat{\mathbf{B}} / \|\hat{\mathbf{B}}\|_F$ 
    10: until Num. of iterations reaches  $N_{\text{Iter}}$ .
        // 3) Update of  $\mathbf{Z}$ 
    11:  $\hat{\mathbf{Z}} \leftarrow \mathcal{S}\left\{ \mathbf{R}_2 + \frac{\hat{\gamma}^* \hat{\mathbf{B}}^{-1} \mathbf{R}_4^T \hat{\mathbf{A}}^{-1}}{1 + |\hat{\gamma}|^2} \right\}$ 
        // 4) Update of  $\gamma$ 
    12:  $\hat{\gamma} \leftarrow \frac{\text{tr}\{(\hat{\mathbf{A}}\hat{\mathbf{Z}}^T\hat{\mathbf{B}})^H\mathbf{R}_4\}}{\|\hat{\mathbf{A}}\hat{\mathbf{Z}}^T\hat{\mathbf{B}}\|_F^2}$ 
    13: until the objective function  $f$  no longer decreases.

```

formation, such as the SNR and the prior distributions of the unknown variables. Consequently, significant performance improvements can be expected by introducing appropriate mathematical models as prior information for the unknown variables and designing the algorithm according to the MMSE criterion. Motivated by this observation, this section develops a Bayesian inference algorithm that explicitly incorporates prior information and performs MMSE estimation.

A. Prior Statistical Modeling of the Unknown Variables

In wireless communication systems, the statistical characteristics and mathematical models of unknown variables can often be inferred from prior observations or estimations, particularly when these variables arise from hardware-induced effects or long-term statistical behaviors. In this subsection, we introduce the statistical quantities and mathematical models explicitly employed in the proposed method.

1) *Complex-Valued Reciprocity Coefficients*: One of the well-established probabilistic models widely adopted to characterize hardware impairments in MIMO arrays is the multiplicative stochastic impairment model [31], [32]. In this model, the residual impairments after compensation are represented by multiplicative amplitude and phase errors. Under this assumption, the complex-valued reciprocity coefficients introduced in (1) are modeled as

$$t_{A,i} = (1 + \epsilon_{TA,i}) e^{j\theta_{TA,i}}, \quad i \in \mathcal{A}, \quad (15a)$$

$$r_{A,i} = (1 + \epsilon_{RA,i}) e^{j\theta_{RA,i}}, \quad i \in \mathcal{A}, \quad (15b)$$

$$t_{B,j} = (1 + \epsilon_{TB,j}) e^{j\theta_{TB,j}}, \quad j \in \mathcal{B}, \quad (15c)$$

$$r_{B,j} = (1 + \epsilon_{RB,j}) e^{j\theta_{RB,j}}, \quad j \in \mathcal{B}, \quad (15d)$$

where $\epsilon_{TA,i}$, $\epsilon_{RA,i}$, $\epsilon_{TB,j}$, and $\epsilon_{RB,j}$ denote the amplitude errors, while $\theta_{TA,i}$, $\theta_{RA,i}$, $\theta_{TB,j}$, and $\theta_{RB,j}$ represent the phase errors, respectively. As discussed in Section II, the dominant sources of the complex-valued reciprocity coefficients at individual antenna elements are phase drift and phase errors induced by different oscillators employed at A and B. Therefore, when modeling the residual amplitude errors after compensation as real-valued Gaussian random variables following $\mathcal{N}(0, \sigma_\epsilon^2)$ [31], we assume that their variance is sufficiently small, *i.e.*, $\sigma_\epsilon \ll 1$.

2) *Measurement Noise:* The observation noise may include, in addition to Gaussian noise originating from thermal noise, spatially colored interference. Moreover, depending on the sampling scheme, temporal correlations may also arise. Therefore, in this paper, in order to appropriately account for such spatio-temporal correlations, the observation noise matrix in (4) is modeled as a circularly symmetric multivariate complex Gaussian random matrix. Assuming that the spatial (column-wise) and temporal (row-wise) correlations are separable and admit a Kronecker representation, the PDFs of the observation noise matrices in (4) are expressed as

$$p_{\mathbf{W}_A^x}(\mathbf{W}_A^x) = \frac{\exp \left[-\text{tr} \left(\bar{\boldsymbol{\Omega}}_A^{-1} \mathbf{W}_A^x \bar{\boldsymbol{\Psi}}_A^{-1} (\mathbf{W}_A^x)^H \right) \right]}{\pi^{M_A M_B} \det(\bar{\boldsymbol{\Omega}}_A)^{M_B} \det(\bar{\boldsymbol{\Psi}}_A)^{M_A}}, \quad (16a)$$

$$p_{\mathbf{W}_B^x}(\mathbf{W}_B^x) = \frac{\exp \left[-\text{tr} \left(\bar{\boldsymbol{\Omega}}_B^{-1} \mathbf{W}_B^x \bar{\boldsymbol{\Psi}}_B^{-1} (\mathbf{W}_B^x)^H \right) \right]}{\pi^{M_B M_A} \det(\bar{\boldsymbol{\Omega}}_B)^{M_A} \det(\bar{\boldsymbol{\Psi}}_B)^{M_B}}, \quad (16b)$$

where $x \in \{0, 1\}$. The spatial correlation matrices at A and B are denoted by $\bar{\boldsymbol{\Omega}}_A \in \mathbb{C}^{M_A \times M_A}$ and $\bar{\boldsymbol{\Omega}}_B \in \mathbb{C}^{M_B \times M_B}$, respectively, while the temporal correlation matrices are denoted by $\bar{\boldsymbol{\Psi}}_A \in \mathbb{C}^{M_B \times M_B}$ and $\bar{\boldsymbol{\Psi}}_B \in \mathbb{C}^{M_A \times M_A}$. For notational simplicity, we further define $\boldsymbol{\Omega}_A \triangleq \bar{\boldsymbol{\Omega}}_A/2$, $\boldsymbol{\Omega}_B \triangleq \bar{\boldsymbol{\Omega}}_B/2$, $\boldsymbol{\Sigma}_A \triangleq \bar{\boldsymbol{\Sigma}}_A/2$, and $\boldsymbol{\Sigma}_B \triangleq \bar{\boldsymbol{\Sigma}}_B/2$ to denote the covariance matrices of the pre-processed measurement noise in (8).

In what follows, these covariance matrices are assumed to be known (or can be accurately estimated *a priori*) and are used in the proposed method. However, if such information is not fully available, the covariance matrices can be constructed using only the available information, and the method can be executed accordingly. Note that the proposed method does not require complete knowledge of the covariance matrices. Even when the full covariance matrices are available, the proposed method can be implemented using only their diagonal elements (*i.e.*, the variance matrices) to reduce the computational complexity. The specific implementation of the proposed method is left to the system designer, depending on practical constraints.

B. Overview

To provide an overview of the proposed algorithm, we present the FG corresponding to the reciprocity calibration task in Fig. 2. In this graph, the square nodes (■) represent factor nodes (FNs) associated with the observations, where f_1 , f_2 , f_3 , and f_4 correspond to (8a), (8b), (8c), and (8d), respectively. The circular nodes (○) represent variable nodes (VNs) associated with the unknown variables in \mathbf{A} and \mathbf{B} . As shown in the figure, the FG centered at f_3 is relatively *sparse*, and since no short

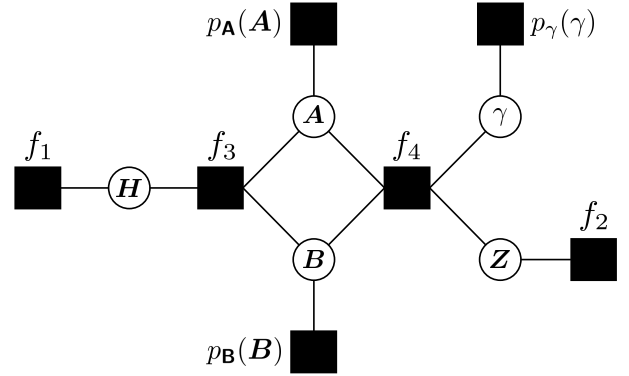


Fig. 2. Illustration of the FG designed for the proposed MMSE algorithm.

When loops exist in the FG, the estimation procedure plays a crucial role in determining the accuracy and stability of the algorithm. The proposed algorithm follows an estimation procedure similar to that of the basic NLS algorithm, in which the estimates of the unknown variables and their associated mean square errors (MSEs), if available, are sequentially propagated over the FG. Finally, by integrating the messages propagated over the FG from all observations, γ is estimated in the MMSE sense.

The key factors that enable performance improvements over the NLS algorithm are threefold: i) the explicit incorporation of the statistical properties of the measurement noise within the Bayesian framework; ii) the use of the prior statistical modeling introduced in (15) for the reciprocity coefficients (*i.e.*, \mathbf{A} and \mathbf{B}) as prior probability distributions; and iii) the estimation of the prior distribution of γ via the method of moments (MoM), followed by MMSE estimation based on the resulting prior. In the following, we describe the details of the proposed algorithm.

C. MMSE Algorithm

1) *Estimation of \mathbf{H} :* From (6a), since \mathbf{H} includes the direct channel \mathbf{G} from A to B, it is practically difficult to assume a statistical prior model for \mathbf{H} . Therefore, as in the NLS algorithm, we use (10) as the point estimate of \mathbf{H} and propagate the associated covariance matrices representing the estimation error information, *i.e.*, $\boldsymbol{\Omega}_B$ and $\boldsymbol{\Psi}_B$.

2) *Estimation of \mathbf{Z} :* Similarly, from (6d), since \mathbf{Z} includes the indirect channels \mathbf{g} and \mathbf{h} via R, it is difficult to assume a statistical prior model for \mathbf{Z} . Therefore, as in the NLS algorithm, we propagate (11) as the point estimate of \mathbf{Z} . Since the estimation error of the rank-one approximation cannot be analytically evaluated, only the estimate is propagated.

3) *Estimation of \mathbf{A} and \mathbf{B} :* Based on (8c), we perform MMSE estimation of \mathbf{A} and \mathbf{B} . To exploit the point estimate of \mathbf{H} and its associated error covariance matrices, together with the prior statistical model introduced in (15), we adopt an iterative alternating estimation approach based on PDA within the Bayesian bilinear inference framework [28]–[30], [33], [34]. To facilitate the understanding of the message update rules, Fig. 3 illustrates in detail the FG composed of the FNs f_3 corresponding to (8c) and the VNs associated with the unknown variables in \mathbf{A} and \mathbf{B} . As shown in the figure, the FG centered at f_3 is relatively *sparse*, and since no short

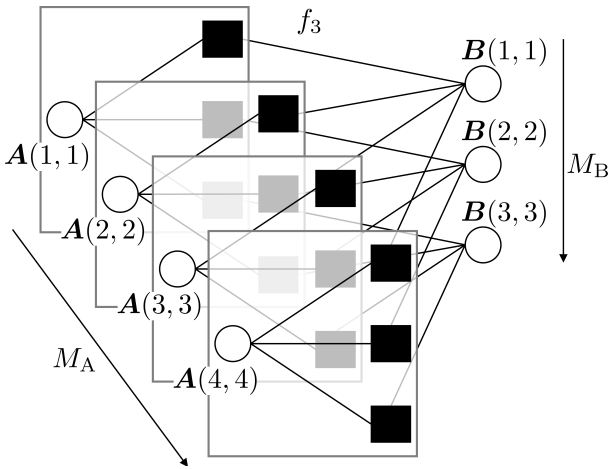


Fig. 3. Illustration of the tripartite FG for bilinear inference of \mathbf{A} and \mathbf{B} with $(M_A, M_B) = (4, 3)$.

loops exist, high-accuracy convergence can be expected with a relatively small number of iterations.

Denoting the estimates of \mathbf{A} and \mathbf{B} by $\hat{\mathbf{A}}$ and $\hat{\mathbf{B}}$, respectively, their MSEs for all $i \in \mathcal{A}$ and $j \in \mathcal{B}$ are given by

$$\hat{v}_{A,i} \triangleq \mathbb{E} [|\tilde{\mathbf{A}}(i,i)|^2], \quad \tilde{\mathbf{A}}(i,i) \triangleq \mathbf{A}(i,i) - \hat{\mathbf{A}}(i,i), \quad (17a)$$

$$\hat{v}_{B,j} \triangleq \mathbb{E} [|\tilde{\mathbf{B}}(j,j)|^2], \quad \tilde{\mathbf{B}}(j,j) \triangleq \mathbf{B}(j,j) - \hat{\mathbf{B}}(j,j), \quad (17b)$$

where $\tilde{\mathbf{A}}$ and $\tilde{\mathbf{B}}$ represent the corresponding estimation error matrices. At the first iteration, the estimates and their MSEs are appropriately initialized as $\hat{\mathbf{A}} = \mathbf{I}_{M_A}$, $\hat{\mathbf{B}} = \mathbf{I}_{M_B}$, and $\hat{v}_{A,i} = \hat{v}_{B,j} = 1$ for all $i \in \mathcal{A}$ and $j \in \mathcal{B}$.

First, to estimate the (i,i) -th entry of \mathbf{A} , we focus on the i -th row of the observation in (8c), which yields the following observation equation:

$$(\mathbf{R}_3^\top)_i = (\mathbf{B}\mathbf{H})_i \mathbf{A}(i,i) + (\mathbf{W}_3^\top)_i \in \mathbb{C}^{M_B \times 1}. \quad (18)$$

Substituting $\mathbf{H} = \hat{\mathbf{H}} + \tilde{\mathbf{H}}$ and $\mathbf{B} = \hat{\mathbf{B}} + \tilde{\mathbf{B}}$ into (18) yields

$$\begin{aligned} (\mathbf{R}_3^\top)_i &= (\hat{\mathbf{B}}\hat{\mathbf{H}})_i \mathbf{A}(i,i) \\ &\quad + (\tilde{\mathbf{B}}\hat{\mathbf{H}})_i \mathbf{A}(i,i) + (\hat{\mathbf{B}}\tilde{\mathbf{H}})_i \mathbf{A}(i,i) \\ &\quad + (\tilde{\mathbf{B}}\tilde{\mathbf{H}})_i \mathbf{A}(i,i) + (\mathbf{W}_3^\top)_i. \end{aligned} \quad (19)$$

In accordance with the central limit theorem (CLT), the terms in the second and third lines of (19) are collectively approximated by a multivariate complex Gaussian random vector. This approximation is referred to as vector Gaussian approximation (VGA) [35]. Accordingly, the conditional PDF of (19), given $\mathbf{A}(i,i)$, can be expressed as

$$\begin{aligned} p_{(\mathbf{R}_3^\top)_i | \mathbf{A}(i,i)} &((\mathbf{R}_3^\top)_i | \mathbf{A}(i,i)) \\ &\propto \exp \left[- \left((\mathbf{R}_3^\top)_i - (\hat{\mathbf{B}}\hat{\mathbf{H}})_i \mathbf{A}(i,i) \right)^\top \mathbf{V}_{A,i}^{-1} \right. \\ &\quad \left. \times \left((\mathbf{R}_3^\top)_i - (\hat{\mathbf{B}}\hat{\mathbf{H}})_i \mathbf{A}(i,i) \right) \right], \end{aligned} \quad (20)$$

where

$$\mathbf{V}_{A,i} \triangleq \mathbb{E} \left[\left((\mathbf{R}_3^\top)_i - (\hat{\mathbf{B}}\hat{\mathbf{H}})_i \mathbf{A}(i,i) \right) \right]$$

$$\begin{aligned} &\times \left((\mathbf{R}_3^\top)_i - (\hat{\mathbf{B}}\hat{\mathbf{H}})_i \mathbf{A}(i,i) \right)^\top \right] \\ &= \Psi_A + \hat{\mathbf{B}}\Omega_B\hat{\mathbf{B}}^\top + \text{diag}(v_{A,i1}, \dots, v_{A,iM_B}), \end{aligned} \quad (21)$$

with

$$v_{A,ij} \triangleq \left(|\hat{\mathbf{H}}(j,i)|^2 + \Omega_B(j,j) \right) \hat{v}_{B,j}. \quad (22)$$

Next, by expanding and rearranging the exponent in (20) and completing the square w.r.t. $\mathbf{A}(i,i)$, we have

$$\begin{aligned} p_{(\mathbf{R}_3^\top)_i | \mathbf{A}(i,i)} &((\mathbf{R}_3^\top)_i | \mathbf{A}(i,i)) \\ &\propto \exp \left[- \frac{|\bar{\mathbf{A}}(i,i) - \mathbf{A}(i,i)|^2}{\bar{v}_{A,i}} \right], \end{aligned} \quad (23)$$

with

$$\bar{\mathbf{A}}(i,i) = \frac{1}{\psi_{A,i}} \left(\hat{\mathbf{B}}\hat{\mathbf{H}} \right)_i^\top \mathbf{V}_{A,i}^{-1} (\mathbf{R}_3^\top)_i, \quad (24a)$$

$$\bar{v}_{A,i} = \frac{1}{\psi_{A,i}}, \quad (24b)$$

where

$$\psi_{A,i} \triangleq \left(\hat{\mathbf{B}}\hat{\mathbf{H}} \right)_i^\top \mathbf{V}_{A,i}^{-1} \left(\hat{\mathbf{B}}\hat{\mathbf{H}} \right)_i. \quad (25)$$

From (23), $\bar{\mathbf{A}}(i,i)$ can be regarded as an additive white Gaussian noise (AWGN) observation of $\mathbf{A}(i,i)$.

Finally, based on the prior statistical model in (15), we consider the prior distribution of $\mathbf{A}(i,i)$. By substituting (1a) and (1b) into (6b), we obtain

$$\begin{aligned} \mathbf{A}(i,i) &= \frac{r_{A,i}}{t_{A,i}} = \frac{(1 + \epsilon_{RA,i}) e^{j\theta_{RA,i}}}{(1 + \epsilon_{TA,i}) e^{j\theta_{TA,i}}} = \left[1 + \frac{\epsilon_i}{1 + \epsilon_{TA,i}} \right] e^{j\theta_i} \\ &\approx e^{j\theta_i} + (1 - \epsilon_{TA,i}) \epsilon_i e^{j\theta_i} \approx e^{j\theta_i} + \epsilon_i e^{j\theta_i} \end{aligned} \quad (26)$$

where $\epsilon_i \triangleq \epsilon_{RA,i} - \epsilon_{TA,i}$ and $\theta_i \triangleq \theta_{RA,i} - \theta_{TA,i}$. The above approximations are obtained under the assumption that $\sigma_\epsilon \ll 1$, where the first approximation uses the first-order expansion $1/(1 + \epsilon_{TA,i}) \approx 1 - \epsilon_{TA,i}$, and the second approximation neglects the second-order term $\epsilon_{TA,i}\epsilon_i$. Since the second term $\epsilon_i e^{j\theta_i}$ has zero mean and a total variance of $2\sigma_\epsilon^2$, its contribution is, with overwhelming probability, sufficiently small compared with that of the first term; therefore, the second term is neglected in this paper. In this case, the prior distribution of $\mathbf{A}(i,i)$ can be modeled using a von Mises distribution based on an exponential-family approximation.

Lemma 1: When $\mathbf{A}(i,i)$ lies on the complex unit circle, the MMSE estimate of $\mathbf{A}(i,i)$ can be computed using the von Mises denoiser as follows:

$$\hat{\mathbf{A}}(i,i) = \eta(\bar{\mathbf{A}}(i,i); \bar{v}_{A,i}) = \frac{I_1(|\zeta_A|)}{I_0(|\zeta_A|)} e^{j \cdot \arg(\zeta_A)}, \quad (27)$$

where $I_n(\cdot)$ denotes the modified Bessel function of the first kind of order n and

$$\zeta_A = \frac{2\bar{\mathbf{A}}(i,i)}{\bar{v}_{A,i}}. \quad (28)$$

The corresponding posterior MSE is given by

$$\hat{v}_{A,i} = \bar{v}_{A,i} \cdot \frac{\partial \eta(\bar{\mathbf{A}}(i,i); \bar{v}_{A,i})}{\partial \bar{\mathbf{A}}(i,i)} = 1 - \left(\frac{I_1(|\zeta_A|)}{I_0(|\zeta_A|)} \right)^2. \quad (29)$$

Proof: The result follows by evaluating the von Mises denoiser in Appendix A at $\beta = 0$ and $r = 1$. ■

In practice, the (unwrapped) phase error variance is generally difficult to estimate accurately, and consequently the corresponding concentration parameter β of the von Mises distribution cannot be reliably determined. Therefore, in this paper, we adopt a non-informative prior on the phase in the denoising process by setting $\beta = 0$, which corresponds to a circularly uniform denoiser.

This completes the MMSE update of $\hat{\mathbf{A}}$.

The estimation of $\mathbf{B}(j, j)$ is performed in exactly the same manner as that of $\mathbf{A}(i, i)$. First, to estimate the (j, j) -th entry of \mathbf{B} , we focus on the j -th column of the observation in (8c), which yields the following observation equation:

$$(\mathbf{R}_3)_j = (\mathbf{A}\mathbf{H}^T)_j \mathbf{B}(j, j) + (\mathbf{W}_3)_j \in \mathbb{C}^{M_A \times 1}. \quad (30)$$

Substituting $\mathbf{H} = \hat{\mathbf{H}} + \tilde{\mathbf{H}}$ and $\mathbf{A} = \hat{\mathbf{A}} + \tilde{\mathbf{A}}$ into (30) yields

$$\begin{aligned} (\mathbf{R}_3)_j &= \left(\hat{\mathbf{A}}\hat{\mathbf{H}}^T \right)_j \mathbf{B}(j, j) \\ &\quad + \left(\tilde{\mathbf{A}}\hat{\mathbf{H}}^T \right)_j \mathbf{B}(j, j) + \left(\hat{\mathbf{A}}\tilde{\mathbf{H}}^T \right)_j \mathbf{B}(j, j) \\ &\quad + \left(\tilde{\mathbf{A}}\tilde{\mathbf{H}}^T \right)_j \mathbf{B}(j, j) + (\mathbf{W}_3)_j. \end{aligned} \quad (31)$$

In accordance with the CLT, the terms in the second and third lines of (31) are collectively approximated by a multivariate complex Gaussian random vector. Accordingly, the conditional PDF of (31), given $\mathbf{B}(j, j)$, can be expressed as

$$\begin{aligned} p_{(\mathbf{R}_3)_j | \mathbf{B}(j, j)} &\left((\mathbf{R}_3)_j | \mathbf{B}(j, j) \right) \\ &\propto \exp \left[- \left((\mathbf{R}_3)_j - \left(\hat{\mathbf{A}}\hat{\mathbf{H}}^T \right)_j \mathbf{B}(j, j) \right)^H \mathbf{V}_{B,j}^{-1} \right. \\ &\quad \left. \times \left((\mathbf{R}_3)_j - \left(\hat{\mathbf{A}}\hat{\mathbf{H}}^T \right)_j \mathbf{B}(j, j) \right) \right], \end{aligned} \quad (32)$$

where

$$\begin{aligned} \mathbf{V}_{B,j} &\triangleq \mathbb{E} \left[\left((\mathbf{R}_3)_j - \left(\hat{\mathbf{A}}\hat{\mathbf{H}}^T \right)_j \mathbf{B}(j, j) \right) \right. \\ &\quad \left. \times \left((\mathbf{R}_3)_j - \left(\hat{\mathbf{A}}\hat{\mathbf{H}}^T \right)_j \mathbf{B}(j, j) \right)^H \right] \\ &= \boldsymbol{\Omega}_A + \hat{\mathbf{A}}\boldsymbol{\Psi}_B\hat{\mathbf{A}}^H + \text{diag}(v_{B,j1}, \dots, v_{B,jM_A}), \end{aligned} \quad (33)$$

with

$$v_{B,ji} \triangleq \left(|\hat{\mathbf{H}}(j, i)|^2 + \boldsymbol{\Psi}_B(i, i) \right) \hat{v}_{A,i}. \quad (34)$$

Next, by expanding and rearranging the exponent in (32) and completing the square w.r.t. $\mathbf{B}(j, j)$, we have

$$\begin{aligned} p_{(\mathbf{R}_3)_j | \mathbf{B}(j, j)} &\left((\mathbf{R}_3)_j | \mathbf{B}(j, j) \right) \\ &\propto \exp \left[- \frac{|\bar{\mathbf{B}}(j, j) - \mathbf{B}(j, j)|^2}{\bar{v}_{B,j}} \right], \end{aligned} \quad (35)$$

with

$$\bar{\mathbf{B}}(j, j) = \frac{1}{\psi_{B,j}} \left(\hat{\mathbf{A}}\hat{\mathbf{H}}^T \right)_j^H \mathbf{V}_{B,j}^{-1} (\mathbf{R}_3)_j, \quad (36a)$$

$$\bar{v}_{B,j} = \frac{1}{\psi_{B,j}}, \quad (36b)$$

where

$$\psi_{B,j} \triangleq \left(\hat{\mathbf{A}}\hat{\mathbf{H}}^T \right)_j^H \mathbf{V}_{B,j}^{-1} \left(\hat{\mathbf{A}}\hat{\mathbf{H}}^T \right)_j. \quad (37)$$

Finally, the prior distribution of $\mathbf{B}(j, j)$ can also be modeled using a von Mises distribution for all $j \in \mathcal{B}$, following exactly the same procedure as in (26). By applying the von Mises denoiser with $\beta = 0$ and $r = 1$, the corresponding MMSE estimates and their associated MSEs can be obtained, *i.e.*,

$$\hat{\mathbf{B}}(j, j) = \eta(\bar{\mathbf{B}}(j, j); \bar{v}_{B,j}) = \frac{I_1(|\zeta_B|)}{I_0(|\zeta_B|)} e^{j \cdot \arg(\zeta_B)}, \quad (38a)$$

$$\bar{v}_{B,j} = \bar{v}_{B,j} \cdot \frac{\partial \eta(\bar{\mathbf{B}}(j, j); \bar{v}_{B,j})}{\partial \bar{\mathbf{B}}(j, j)} = 1 - \left(\frac{I_1(|\zeta_B|)}{I_0(|\zeta_B|)} \right)^2, \quad (38b)$$

where

$$\zeta_B = \frac{2\bar{\mathbf{B}}(j, j)}{\bar{v}_{B,j}}. \quad (39)$$

4) *Estimation of γ :* All estimates obtained in the preceding steps are substituted into (8d), which yields

$$\begin{aligned} \mathbf{R}_4 &= \gamma \left(\hat{\mathbf{A}} + \tilde{\mathbf{A}} \right) \hat{\mathbf{Z}}^T \left(\hat{\mathbf{B}} + \tilde{\mathbf{B}} \right) + \mathbf{W}_4 \\ &= \gamma \underbrace{\hat{\mathbf{A}}\hat{\mathbf{Z}}^T\hat{\mathbf{B}}}_{\triangleq \hat{\mathbf{D}}} + \gamma \underbrace{\left(\tilde{\mathbf{A}}\hat{\mathbf{Z}}^T\hat{\mathbf{B}} + \hat{\mathbf{A}}\hat{\mathbf{Z}}^T\tilde{\mathbf{B}} + \tilde{\mathbf{A}}\hat{\mathbf{Z}}^T\tilde{\mathbf{B}} \right)}_{\triangleq \tilde{\mathbf{D}}} + \mathbf{W}_4 \\ &= \gamma \hat{\mathbf{D}} + \gamma \tilde{\mathbf{D}} + \mathbf{W}_4, \end{aligned} \quad (40)$$

where we assume $\hat{\mathbf{Z}} \approx \mathbf{Z}$. For MMSE estimation of γ , (40) is rewritten in the following vectorized form:

$$\text{vec}(\mathbf{R}_4) = \underbrace{\text{vec}(\hat{\mathbf{D}})}_{\triangleq \hat{\mathbf{d}}} \gamma + \underbrace{\text{vec}(\tilde{\mathbf{D}})}_{\triangleq \tilde{\mathbf{d}}} \gamma + \underbrace{\text{vec}(\mathbf{W}_4)}_{\triangleq \mathbf{w}_4}. \quad (41)$$

In accordance with the CLT, the second and third terms in (41) are collectively approximated by a multivariate complex Gaussian random vector. Accordingly, the conditional PDF of (41), given \mathbf{R}_4 , can be expressed as

$$\begin{aligned} p_{\text{vec}(\mathbf{R}_4) | \gamma} &\left(\text{vec}(\mathbf{R}_4) | \gamma \right) \\ &\propto \exp \left[- \left(\text{vec}(\mathbf{R}_4) - \hat{\mathbf{d}}\gamma \right)^H \mathbf{V}_\gamma^{-1} \left(\text{vec}(\mathbf{R}_4) - \hat{\mathbf{d}}\gamma \right) \right], \end{aligned} \quad (42)$$

where

$$\begin{aligned} \mathbf{V}_\gamma &\triangleq \mathbb{E} \left[\left(\text{vec}(\mathbf{R}_4) - \hat{\mathbf{d}}\gamma \right) \left(\text{vec}(\mathbf{R}_4) - \hat{\mathbf{d}}\gamma \right)^H \right] \\ &= \boldsymbol{\Sigma}_A + \mathbf{V}_\gamma^D, \end{aligned} \quad (43)$$

with $\boldsymbol{\Sigma}_A \triangleq \boldsymbol{\Psi}_A \otimes \boldsymbol{\Omega}_A$, $\mathbf{V}_\gamma^D \triangleq \text{diag}(v_{\gamma,11}, \dots, v_{\gamma,M_AM_B})$,

$$\begin{aligned} v_{\gamma,ij} &\triangleq \phi_\gamma |\hat{\mathbf{Z}}(j, i)|^2 \\ &\quad \times \left(\hat{v}_{A,i} |\hat{\mathbf{B}}(j, j)|^2 + |\hat{\mathbf{A}}(i, i)|^2 \hat{v}_{B,j} + \hat{v}_{A,i} \hat{v}_{B,j} \right), \end{aligned} \quad (44)$$

and $\phi_\gamma \triangleq \mathbb{E}[|\gamma|^2]$.

By expanding and rearranging the exponent in (42) and completing the square w.r.t. γ , we have

$$p_{\text{vec}(\mathbf{R}_4) | \gamma} \left(\text{vec}(\mathbf{R}_4) | \gamma \right) \propto \exp \left[- \frac{|\bar{\gamma} - \gamma|^2}{\bar{v}_\gamma} \right], \quad (45)$$

with

$$\bar{\gamma} = \frac{\hat{\mathbf{d}}^H \mathbf{V}_\gamma^{-1} \text{vec}(\mathbf{R}_4)}{\psi_\gamma}, \quad \bar{v}_\gamma = \frac{1}{\psi_\gamma}, \quad (46)$$

where

$$\psi_\gamma \triangleq \hat{\mathbf{d}}^H \mathbf{V}_\gamma^{-1} \hat{\mathbf{d}}. \quad (47)$$

Since ϕ_γ used in (44) is generally unavailable, its treatment requires further discussion. Ideally, the true long-term statistic $\phi_\gamma \triangleq \mathbb{E}[|\gamma|^2]$ is available during system setup, in which case it can be directly used. When ϕ_γ is unknown, several alternatives can be considered. The simplest approach is to operate the system with $\phi_\gamma = 1$, noting that the ultimate goal of calibration is to achieve $\alpha = \beta$. This corresponds to determining the reliability of the estimate solely based on the SNR. In this paper, as a more adaptive alternative, we approximate the true long-term statistic ϕ_γ by an instantaneous estimate of $|\gamma|^2$, obtained via the MoM described below.

Lemma 2: A consistent estimate of $|\gamma|^2$ based on the observation in (8d) can be obtained via the method of moments (MoM) as follows:

$$|\tilde{\gamma}|^2 = \frac{|q|^2 - u}{u^2 + s}, \quad (48)$$

where

$$q \triangleq \hat{\mathbf{d}}^H \Sigma_A^{-1} \text{vec}(\mathbf{R}_4), \quad (49a)$$

$$u \triangleq \hat{\mathbf{d}}^H \Sigma_A^{-1} \hat{\mathbf{d}}, \quad (49b)$$

$$s \triangleq \hat{\mathbf{d}}^H \Sigma_A^{-1} \mathbf{V}_\gamma^D \Sigma_A^{-1} \hat{\mathbf{d}}. \quad (49c)$$

Proof: From the definition in (49a) and the vectorized observation model in (41), we have

$$q = \underbrace{\hat{\mathbf{d}}^H \Sigma_A^{-1} \hat{\mathbf{d}}}_u \gamma + \underbrace{\hat{\mathbf{d}}^H \Sigma_A^{-1} \tilde{\mathbf{d}}}_\kappa \gamma + \underbrace{\hat{\mathbf{d}}^H \Sigma_A^{-1} \mathbf{w}_4}_\kappa. \quad (50)$$

Since $\mathbb{E}[\tilde{\mathbf{d}}] = \mathbb{E}[\mathbf{w}_4] = \mathbf{0}$, it follows that $\mathbb{E}[\kappa_1] = \mathbb{E}[\kappa_2] = 0$. Moreover,

$$\mathbb{E}[|\kappa_1|^2] = \hat{\mathbf{d}}^H \Sigma_A^{-1} \mathbf{V}_\gamma^D \Sigma_A^{-1} \hat{\mathbf{d}} = s, \quad (51a)$$

$$\mathbb{E}[|\kappa_2|^2] = \hat{\mathbf{d}}^H \Sigma_A^{-1} \hat{\mathbf{d}} = u. \quad (51b)$$

By squaring both sides of (50) and taking the expectation, we obtain

$$\mathbb{E}[|q|^2] = (u^2 + s) |\gamma|^2 + u, \quad (52)$$

where we use the independence of $\tilde{\mathbf{d}}$ and \mathbf{w}_4 . Equating the theoretical moment $\mathbb{E}[|q|^2]$ with its single-sample counterpart $|q|^2$ and solving for $|\gamma|^2$ yields (48). \blacksquare

Finally, since an estimate of $|\gamma|$ is obtained by taking the square root of (48), we can model the prior distribution of γ as a circularly uniform distribution on the complex circle with radius $|\tilde{\gamma}|$. By applying the von Mises denoiser with $\beta = 0$ and $r = |\tilde{\gamma}|$, the corresponding MMSE estimate and its associated MSE can be obtained, *i.e.*,

$$\hat{\gamma} = \eta(\bar{\gamma}; \bar{v}_\gamma) = |\tilde{\gamma}| \frac{I_1(|\zeta_\gamma|)}{I_0(|\zeta_\gamma|)} e^{j \cdot \arg(\zeta_\gamma)}, \quad (53a)$$

$$\hat{v}_\gamma = \bar{v}_\gamma \cdot \frac{\partial \eta(\bar{\gamma}; \bar{v}_\gamma)}{\partial \bar{\gamma}} = |\tilde{\gamma}|^2 \left(1 - \left(\frac{I_1(|\zeta_\gamma|)}{I_0(|\zeta_\gamma|)} \right)^2 \right), \quad (53b)$$

where

$$\zeta_\gamma = \frac{2|\tilde{\gamma}|}{\bar{v}_\gamma} \bar{\gamma}. \quad (54)$$

With the above derivations, the proposed algorithm is specified and summarized in Algorithm 3.

Algorithm 3 : MMSE-based calibration algorithm

Input: $\mathbf{R}_1, \mathbf{R}_2, \mathbf{R}_3, \mathbf{R}_4, (\Omega_A, \Omega_B, \Psi_A, \Psi_B$ if available)

Output: $\hat{\mathbf{H}}, \hat{\mathbf{Z}}, \hat{\mathbf{A}}, \hat{\mathbf{B}}, \hat{\gamma}$

// 1) Estimation of \mathbf{H}

1: $\hat{\mathbf{H}} \leftarrow \mathbf{R}_1$

// 2) Estimation of \mathbf{Z}

2: $\hat{\mathbf{Z}} \leftarrow \mathcal{S}\{\mathbf{R}_2\}$

// 3) Estimation of \mathbf{A} and \mathbf{B}

3: $\hat{\mathbf{A}} \leftarrow \mathbf{I}_{M_A}, \hat{\mathbf{B}} \leftarrow \mathbf{I}_{M_B}$ Initialization

4: $\forall i \in \mathcal{A}, \forall j \in \mathcal{B} : \hat{v}_{A,i} \leftarrow 1, \hat{v}_{B,j} \leftarrow 1$

5: **repeat**

6: $\forall i \in \mathcal{A} : \text{Compute } \mathbf{V}_{A,i} \text{ using (21).}$

7: $\forall i \in \mathcal{A} : \psi_{A,i} \leftarrow (\hat{\mathbf{B}} \hat{\mathbf{H}})_i^H \mathbf{V}_{A,i}^{-1} (\hat{\mathbf{B}} \hat{\mathbf{H}})_i$

8: $\forall i \in \mathcal{A} : \bar{\mathbf{A}}(i, i) \leftarrow \frac{1}{\psi_{A,i}} (\hat{\mathbf{B}} \hat{\mathbf{H}})_i^H \mathbf{V}_{A,i}^{-1} (\mathbf{R}_3)_i$

9: $\forall i \in \mathcal{A} : \bar{v}_{A,i} \leftarrow \frac{1}{\psi_{A,i}}$

10: $\forall i \in \mathcal{A} : \zeta_A \leftarrow \frac{1}{\bar{v}_{A,i}} \bar{\mathbf{A}}(i, i)$

11: $\forall i \in \mathcal{A} : \hat{\mathbf{A}}(i, i) \leftarrow \frac{I_1(|\zeta_A|)}{I_0(|\zeta_A|)} e^{j \cdot \arg(\zeta_A)}$

12: $\forall i \in \mathcal{A} : \hat{v}_{A,i} \leftarrow \left(1 - \left(\frac{I_1(|\zeta_A|)}{I_0(|\zeta_A|)} \right)^2 \right)$

13: $\forall j \in \mathcal{B} : \text{Compute } \mathbf{V}_{B,j} \text{ using (33).}$

14: $\forall j \in \mathcal{B} : \psi_{B,j} \leftarrow (\hat{\mathbf{A}} \hat{\mathbf{H}}^T)_j^H \mathbf{V}_{B,j}^{-1} (\hat{\mathbf{A}} \hat{\mathbf{H}}^T)_j$

15: $\forall j \in \mathcal{B} : \bar{\mathbf{B}}(j, j) \leftarrow \frac{1}{\psi_{B,j}} (\hat{\mathbf{A}} \hat{\mathbf{H}}^T)_j^H \mathbf{V}_{B,j}^{-1} (\mathbf{R}_3)_j$

16: $\forall j \in \mathcal{B} : \bar{v}_{B,j} \leftarrow \frac{1}{\psi_{B,j}}$

17: $\forall j \in \mathcal{B} : \zeta_B \leftarrow \frac{1}{\bar{v}_{B,j}} \bar{\mathbf{B}}(j, j)$

18: $\forall j \in \mathcal{B} : \hat{\mathbf{B}}(j, j) \leftarrow \frac{I_1(|\zeta_B|)}{I_0(|\zeta_B|)} e^{j \cdot \arg(\zeta_B)}$

19: $\forall j \in \mathcal{B} : \hat{v}_{B,j} \leftarrow \left(1 - \left(\frac{I_1(|\zeta_B|)}{I_0(|\zeta_B|)} \right)^2 \right)$

20: **until** Num. of iterations reaches N_{Iter}

// 4) Estimation of γ

21: Compute \mathbf{V}_γ and \mathbf{V}_γ^D using (43).

22: $\hat{\mathbf{d}} \leftarrow \text{vec}(\hat{\mathbf{A}} \hat{\mathbf{Z}}^T \hat{\mathbf{B}}), \quad q \leftarrow \hat{\mathbf{d}}^H \Sigma_A^{-1} \text{vec}(\mathbf{R}_4)$

23: $u \leftarrow \hat{\mathbf{d}}^H \Sigma_A^{-1} \hat{\mathbf{d}}, \quad s \leftarrow \hat{\mathbf{d}}^H \Sigma_A^{-1} \mathbf{V}_\gamma^D \Sigma_A^{-1} \hat{\mathbf{d}}$

24: $|\tilde{\gamma}|^2 \leftarrow \frac{|q|^2 - u}{u^2 + s}$

25: $\psi_\gamma \leftarrow \hat{\mathbf{d}}^H \mathbf{V}_\gamma^{-1} \hat{\mathbf{d}}$

26: $\bar{\gamma} \leftarrow \frac{1}{\psi_\gamma} \hat{\mathbf{d}}^H \mathbf{V}_\gamma^{-1} \text{vec}(\mathbf{R}_4)$

27: $\zeta_\gamma = \frac{2|\tilde{\gamma}|}{\bar{v}_\gamma} \bar{\gamma}$

28: $\hat{\gamma} \leftarrow |\tilde{\gamma}| \frac{I_1(|\zeta_\gamma|)}{I_0(|\zeta_\gamma|)} e^{j \cdot \arg(\zeta_\gamma)}$

D. Complexity Analysis

Finally, we evaluate the computational complexity of the proposed MMSE algorithm (Algorithm 3) in comparison with the basic NLS (Algorithm 1) and the alternating-optimization NLS (Algorithm 2). For all methods, the estimation of \mathbf{Z} requires computing the best rank-one approximation of \mathbf{R}_2 via the operator $\mathcal{S}\{\cdot\}$, which, in the worst case, generally involves a full singular value decomposition (SVD). Hence, the computational complexity is on the order of

$$C_S = \mathcal{O}(M_A M_B \min\{M_A, M_B\}). \quad (55)$$

However, in practice, Krylov subspace methods such as the power method or the Lanczos algorithm can be employed to efficiently compute the largest singular value and its corresponding singular vectors iteratively, which reduces the computational cost to $\mathcal{O}(\tau M_A M_B)$, where τ denotes the number of iterations and is typically a small constant in practice.

1) *NLS (Algorithm 1)*: For the basic NLS algorithm, the dominant computational cost arises from the rank-one approximation for estimating \mathbf{Z} and the N_{Iter} alternating updates for estimating \mathbf{A} and \mathbf{B} . Since \mathbf{A} and \mathbf{B} are diagonal matrices, their updates reduce to inner-product computations and element-wise operations; hence, the computational complexity per iteration for updating $\hat{\mathbf{A}}$ and $\hat{\mathbf{B}}$ is on the order of $\mathcal{O}(M_A M_B)$. Moreover, the final estimation of γ is also performed using only element-wise operations and trace computations, which requires $\mathcal{O}(M_A M_B)$ complexity. Therefore, the overall computational complexity is given by

$$C_{\text{NLS}} = \mathcal{O}(C_S + N_{\text{Iter}} M_A M_B). \quad (56)$$

2) *Alternating-optimization. NLS (Algorithm 2)*: The alternating-optimization NLS first obtains an initial estimate using the basic NLS, and then improves the estimation accuracy through alternating optimization with outer iterations. In each outer iteration, the rank-one approximation appears once for updating $\hat{\mathbf{Z}}$, and the inner iterations for updating $\hat{\mathbf{A}}$ and $\hat{\mathbf{B}}$ are repeated N_{Iter} times. Compared with Algorithm 1, the newly introduced update of $\hat{\mathbf{H}}$ is formulated as a matrix inversion based on the least-squares criterion. However, since \mathbf{A} and \mathbf{B} are diagonal matrices, this operation can be implemented element-wise, which reduces the computational complexity to the order of $\mathcal{O}(M_A M_B)$. Including the cost of the initial estimation by the basic NLS, the overall computational complexity is given by

$$C_{\text{AO-NLS}} = \mathcal{O}((N_{\text{opt}} + 1)(C_S + N_{\text{Iter}} M_A M_B)), \quad (57)$$

where N_{opt} denotes the number of outer iterations required for convergence, *i.e.*, until the decrease in the cost function becomes sufficiently small.

3) *MMSE (Algorithm 3)*: In Algorithm 3, the dominant factors determining the computational complexity are the estimation of \mathbf{A} and \mathbf{B} , as well as the estimation of γ . Note that the denoising operations based on the von Mises denoiser are all performed in a scalar-wise manner and can be efficiently implemented using table lookups of the modified Bessel functions. As discussed above, the proposed MMSE algorithm is generalized to incorporate knowledge of the covariance matrices of the observation noise, and its computational complexity largely depends on how much of this information is exploited in the estimation process. In the following, we evaluate two cases: i) using the full covariance matrices in (16), and ii) using only their diagonal elements (*i.e.*, the variances).

i) **Full covariance matrices**: When the full covariance matrix is utilized, the estimation of \mathbf{A} involves matrix inversions of $\mathbf{V}_{A,i}$ for all $i \in \mathcal{A}$, which results in a computational complexity on the order of $\mathcal{O}(M_A M_B^3)$ per update. Similarly, the update of $\hat{\mathbf{B}}$ requires $\mathcal{O}(M_A^3 M_B)$ operations. These alternating updates are repeated N_{Iter} times. Furthermore, the estimation of γ involves a matrix inversion of

$\mathbf{V}_\gamma \in \mathbb{C}^{M_A M_B \times M_A M_B}$, whose computational complexity is on the order of $\mathcal{O}(M_A^3 M_B^3)$. Therefore, the overall computational complexity of the algorithm is given by

$$\begin{aligned} & C_{\text{MMSE}} \\ &= \mathcal{O}(C_S + N_{\text{Iter}} (M_A M_B^3 + M_A^3 M_B) + M_A^3 M_B^3). \end{aligned} \quad (58)$$

Since the covariance matrices represent long-term statistics, they typically vary slowly over time. Hence, the matrix inversion associated with Σ_A can be regarded as an offline operation and excluded from the online complexity evaluation. In this case, the estimation of γ is dominated by matrix–vector multiplications, and the overall computational complexity can be reduced to

$$\begin{aligned} & C_{\text{MMSE}} \\ &= \mathcal{O}(C_S + N_{\text{Iter}} (M_A M_B^3 + M_A^3 M_B) + M_A^2 M_B^2). \end{aligned} \quad (59)$$

It is worth noting that achieving improved estimation accuracy by exploiting the full covariance information inevitably comes at the cost of increased computational complexity.

ii) **Diagonal variance matrices**: When only the diagonal elements of the covariance matrices are used, the matrix inversions of $\mathbf{V}_{A,i}$, $\mathbf{V}_{B,j}$, and \mathbf{V}_γ are simplified to element-wise reciprocal operations. Consequently, the per-iteration complexity for estimating \mathbf{A} and \mathbf{B} , as well as for estimating γ , is reduced to $\mathcal{O}(M_A M_B)$, which is comparable to that of the NLS-based algorithms. Therefore, in this case, the computational complexity is given by

$$C_{\text{MMSE}} = \mathcal{O}(C_S + N_{\text{Iter}} M_A M_B). \quad (60)$$

In other words, when the prior knowledge of the observation noise is limited to the variance matrix, the proposed MMSE algorithm operates with a computational complexity on the same order as that of the basic NLS algorithm.

V. PERFORMANCE ASSESSMENT

To verify the effectiveness of the proposed method, computer simulations are conducted. As an illustrative example, following [27], the system parameters listed in Table I are adopted. The vectors \mathbf{h} and \mathbf{g} are chosen as random columns of the $M_A \times M_A$ and $M_B \times M_B$ discrete Fourier transform (DFT) matrices, respectively, which model LoS propagation between A and R, and between R and B. The direct channel \mathbf{G} between A and B, excluding R, consists of independent and identically distributed (i.i.d.) $\mathcal{CN}(0, 1)$ entries, modeling Rayleigh fading. The diagonal elements of \mathbf{T}_A , \mathbf{R}_A , \mathbf{T}_B , and \mathbf{R}_B in (1) have unit magnitude and phases uniformly distributed over $[-\pi, \pi]$ [36]. This setting corresponds to a phase-dominant non-reciprocity scenario, where amplitude mismatches are negligible and non-reciprocity is mainly caused by phase drift/phase errors, as explained in Section II. The entries of the noise matrices \mathbf{W}_B^0 , \mathbf{W}_A^0 , \mathbf{W}_B^1 , and \mathbf{W}_A^1 in (4) are independently drawn from $\mathcal{CN}(0, \sigma^2)$, where the inverse noise variance, $1/\sigma^2$, represents the SNR measured at any antenna of B when a single antenna of A transmits with unit-power and the repeater R is inactive. This corresponds to modeling the observation noise as AWGN, which is equivalent to setting $\bar{\Omega}_A = \bar{\Psi}_B = \sigma^2 \mathbf{I}_{M_A}$ and $\bar{\Omega}_B = \bar{\Psi}_A = \sigma^2 \mathbf{I}_{M_B}$ in (16).

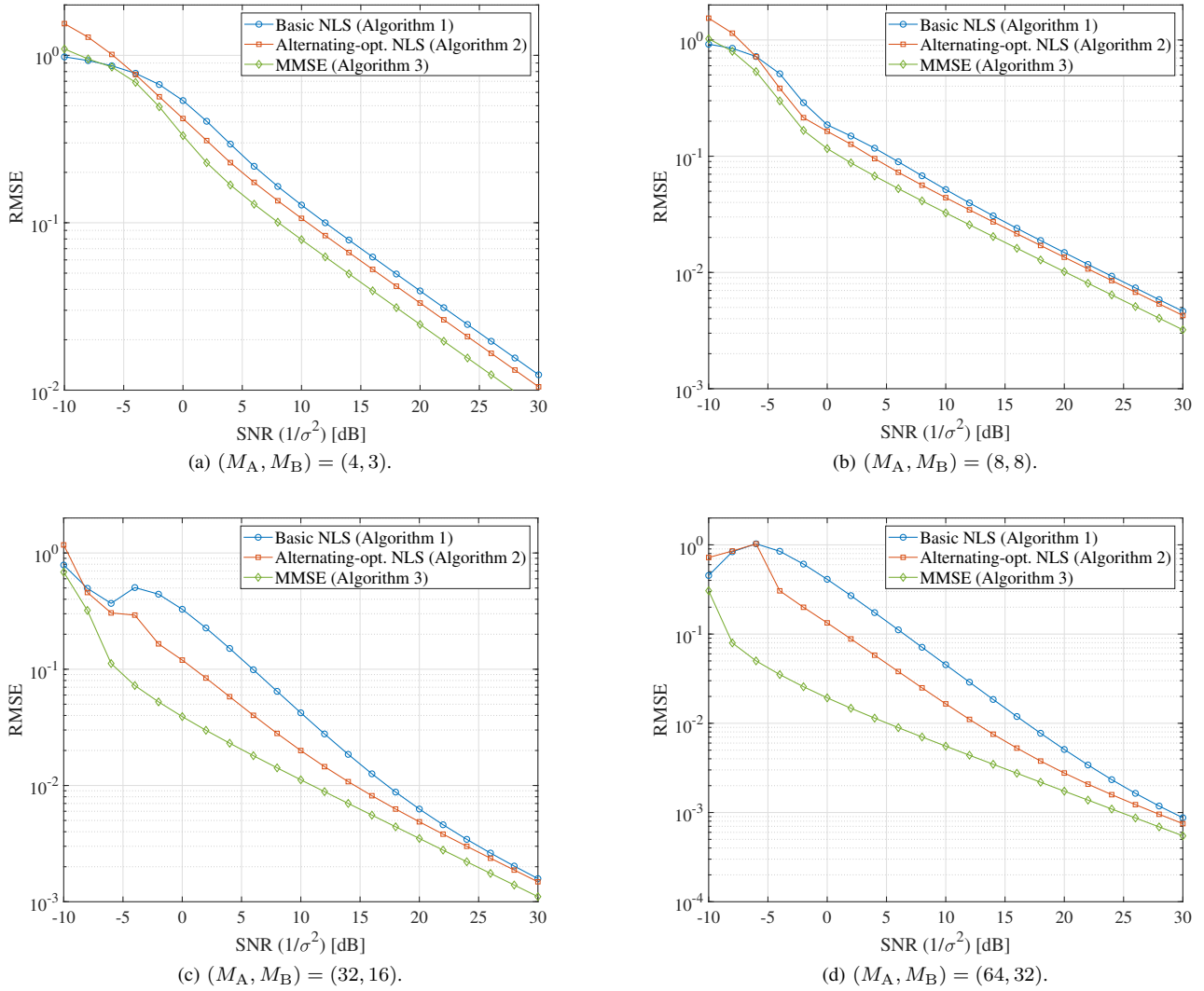


Fig. 4. Root mean square error (RMSE) of $\hat{\gamma}$ for different antenna configurations.

TABLE I
SIMULATION PARAMETERS

Parameter	Symbol	Value
Forward gain of the repeater	$ \alpha ^2$ [dB]	10
Reverse gain of the repeater	$ \beta ^2$ [dB]	10
Num. of iterations for \mathbf{A}, \mathbf{B} estimation	N_{Iter}	100
Num. of simulation trials	-	10^5

Under the above settings, it is worth noting that the amount of additional prior information exploited by the proposed MMSE algorithm, compared with the NLS-based methods, is minimal, and its computational complexity is of the same order, as indicated in (60).

A. RMSE Performance

Fig. 4 shows the RMSE of $\hat{\gamma}$ as a function of the SNR for the NLS (Algorithm 1), the alternating-optimization NLS (Algorithm 2), and the proposed MMSE (Algorithm 3). To evaluate the impact of the transmit and receive array sizes, four antenna configurations are considered, namely, $(M_A, M_B) = (4, 3)$, $(8, 8)$, $(32, 16)$, and $(64, 32)$. These results clearly highlight

the fundamental differences between the proposed MMSE algorithm and the existing NLS-based methods.

We first focus on the results for relatively small array sizes shown in Figs. 4(a) and 4(b). In the moderate-to-high SNR regime ($\text{SNR} > 5$ dB), all methods are observed to operate stably. For both the NLS and MMSE-based methods, the RMSE decreases approximately linearly with SNR (e.g., a 20 dB increase in SNR leads to roughly a tenfold reduction in RMSE). This behavior can be explained by the fact that the observation noise is Gaussian and the curvature of the log-likelihood function, *i.e.*, the Fisher information, scales proportionally with SNR. In this regime, the local linearization around the true parameter is valid and the Jacobian matrix is full rank, so that the error scaling of the NLS and MMSE estimators coincides, which is consistent with estimation theory. Nevertheless, since the MMSE estimator exploits the prior statistical modeling as well as the noise variance, it consistently achieves better performance in terms of the constant factor. Specifically, the proposed MMSE method provides approximately 4 dB and 2 dB performance gains over the basic NLS and the alternating-optimization NLS, respectively.

It is also worth noting that the alternating-optimization NLS incurs an additional computational cost proportional to N_{opt} , whereas the proposed MMSE method achieves these gains with a computational complexity comparable to that of the basic NLS.

We next consider the results for relatively large array sizes shown in Figs. 4(c) and 4(d), where the difference between NLS and MMSE becomes more pronounced. As the array dimension increases, the NLS estimator, which essentially solves a geometric optimization problem, becomes increasingly sensitive to high-dimensional effects. In particular, the singular value distribution of the Jacobian matrix tends to deteriorate, and the curvature of the log-likelihood function becomes small along many directions. As a consequence, the error covariance matrix of the NLS estimator becomes ill-conditioned, and the resulting RMSE no longer scales proportionally with the SNR, not even in the high-SNR regime. Since calibration tasks are typically performed under low-SNR conditions, such behavior of the NLS estimator is undesirable in practical systems.

In contrast, for the MMSE estimator, the prior distribution introduces a regularization term into the Hessian matrix, which keeps the estimation problem well-conditioned. As a result, even in high-dimensional and low-SNR regimes, the RMSE exhibits a stable behavior and remains close to the ideal $1/\text{SNR}$ scaling. Moreover, as the dimensionality increases, the posterior distribution tends to concentrate due to the concentration-of-measure phenomenon, which leads to a self-averaging effect that mitigates the impact of local nonlinearities and noise fluctuations. This effect further stabilizes the MMSE estimator and improves the accuracy of the Gaussian approximations based on the CLT, which are extensively employed in the proposed algorithm. Consequently, the proposed MMSE method follows the theoretical $1/\text{SNR}$ scaling even at low SNR¹. In particular, for the largest array configuration in Fig. 4(d), the proposed MMSE method achieves performance gains of approximately 14 dB and 10 dB over the basic NLS and the alternating-optimization NLS, respectively, at $\text{RMSE} = 10^{-1}$, indicating that large-scale arrays are especially beneficial for the proposed MMSE approach.

B. Convergence Behavior of \mathbf{A} and \mathbf{B} Estimation

To further clarify the behavior of the proposed algorithms, we next investigate their iterative convergence by focusing on the bilinear inference of \mathbf{A} and \mathbf{B} . Fig. 5 shows the RMSE of $\hat{\gamma}$ as a function of the number of iterations N_{Iter} . For the relatively small array size shown in Fig. 5(a), the estimation performance of the basic NLS improves monotonically with the number of iterations and eventually converges to a stable solution. However, even in the high-SNR regime (SNR = 20 dB), approximately 20 iterations are required to reach convergence. For the large array configuration shown in Fig. 5(b), the convergence behavior of the NLS deteriorates significantly in the low-SNR regime. In this case, increasing the number of iterations does not lead to substantial performance

¹Although these numerical results are consistent with theoretical scaling laws, deriving a rigorous closed-form Cramér-Rao lower bound (CRLB) for the present bilinear inference problem with latent variables is nontrivial and is left for future work.

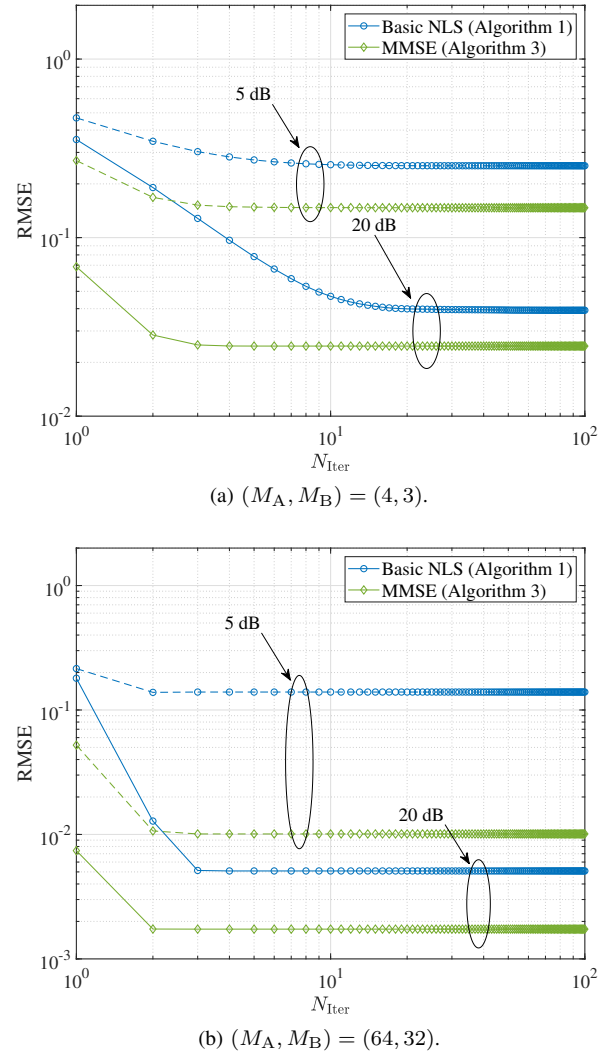


Fig. 5. Iterative convergence behavior of NLS-based and MMSE-based reciprocity calibration algorithms.

improvements, and the estimation error often saturates at a relatively high level. This phenomenon can be attributed to the intrinsic nonconvexity of the bilinear LS problem and the high-dimensional geometric effects discussed previously.

In contrast, the proposed MMSE method exhibits a fundamentally different convergence behavior. Since the bilinear inference step is formulated as a sequence of Bayesian updates, each iteration effectively refines the posterior distribution by incorporating additional statistical information. As a result, the estimation performance improves steadily with the number of iterations and converges rapidly, typically within 4 iterations for all considered scenarios. In particular, for the large-scale array shown in Fig. 5(b), an even faster convergence is observed due to the self-averaging effect induced by high dimensionality, which is consistent with the results discussed in the previous subsection.

VI. CONCLUSION

This paper proposed a novel Bayesian reciprocity calibration framework for repeater-assisted MIMO. By explicitly incorpo-

rating a prior statistical model of the reciprocity coefficients and the measurement noise, the proposed method enables a principled Bayesian formulation of the calibration problem, resulting in a robust estimation framework. To effectively exploit the phase structure of the reciprocity coefficients, a von Mises denoiser was developed. In addition, a MoM-based approach was introduced to adaptively estimate the required second-order statistics, avoiding the need for unavailable long-term prior information. Simulation results demonstrated that the proposed MMSE algorithm can significantly outperform existing deterministic NLS-based methods in terms of estimation accuracy, at comparable computational complexity. Moreover, the proposed method exhibits fast and stable convergence and remains robust w.r.t. both the array size and the SNR. Overall, it provides an efficient and practically implementable solution for reciprocity calibration in repeater-assisted MIMO systems.

APPENDIX A DENOISER DESIGN FOR VON MISES PRIOR DISTRIBUTION

Consider the following AWGN observation model:

$$y = x + w, \quad w \sim \mathcal{CN}(0, v), \quad (61)$$

where $x \triangleq r e^{j\theta}$ is a point on the circle of radius r in the complex plane, and its phase θ follows the von Mises distribution

$$p_\theta(\theta) = \frac{1}{2\pi I_0(\beta)} \exp(\beta \cos(\theta - \mu)), \quad (62)$$

with $I_n(\cdot)$ denoting the modified Bessel function of the first kind of order n and the parameters μ and β representing the location and concentration of the distribution, respectively. These parameters are analogous to the mean and precision of a Gaussian distribution.

Under the assumption that the observation y and the prior distribution in (62) are known, we derive the MMSE estimator of x based on the model in (61) as

$$\hat{x}_{\text{MMSE}} = \mathbb{E}[x|y] = r \cdot \mathbb{E}[e^{j\theta}|y]. \quad (63)$$

First, the likelihood function for a given observation y is given by

$$\begin{aligned} p_{y|\theta}(y|\theta) &= \frac{1}{\pi v} \exp\left[-\frac{|y - r e^{j\theta}|^2}{v}\right] \\ &\propto \exp\left[\frac{2r}{v} \Re\{y e^{-j\theta}\}\right]. \end{aligned} \quad (64)$$

Next, using Bayes' rule, the posterior distribution can be expressed as

$$\begin{aligned} p_{\theta|y}(\theta|y) &\propto p_{y|\theta}(y|\theta)p_\theta(\theta) \\ &\propto \exp\left[\frac{2r}{v} \Re\{y e^{-j\theta}\} + \beta \cos(\theta - \mu)\right] \\ &= \exp\left[\Re\left\{\left(\frac{2r}{v}y + \beta e^{j\mu}\right) e^{-j\theta}\right\}\right] \\ &= \exp\left[\Re\{\zeta(y, r, v, \mu, \beta) e^{-j\theta}\}\right], \end{aligned} \quad (65)$$

where

$$\zeta(y, r, v, \mu, \beta) \triangleq \frac{2r}{v}y + \beta e^{j\mu}. \quad (66)$$

From (65) and (66), the posterior distribution can be again represented by the von Mises distribution as

$$p_{\theta|y}(\theta|y) = \frac{1}{2\pi I_0(|\zeta|)} \exp[|\zeta| \cos(\theta - \arg(\zeta))]. \quad (67)$$

Finally, substituting (67) into (63) yields

$$\begin{aligned} \hat{x}_{\text{MMSE}} &= r \cdot \mathbb{E}[e^{j\theta}|y] \\ &= r \cdot \int_0^{2\pi} e^{j\theta} \cdot p_{\theta|y}(\theta|y) d\theta \\ &= \frac{r e^{j \arg(\zeta)}}{I_0(|\zeta|)} \cdot \underbrace{\frac{1}{2\pi} \int_0^{2\pi} e^{j\theta} \exp[|\zeta| \cos(\theta)] d\theta}_{=I_1(|\zeta|)} \\ &= r \frac{I_1(|\zeta|)}{I_0(|\zeta|)} e^{j \arg(\zeta)} \triangleq \eta(y; v), \end{aligned} \quad (68)$$

where the function η represents the MMSE solution in (61) expressed as a function of y and v , and such a formulation is often referred to as a *Bayes-optimal denoiser (BOD)*. The mathematical manipulations involving the modified Bessel functions are provided in Appendix B.

For the BOD, it is known that the following identity holds between the MMSE solution and its MSE:

$$v \cdot \frac{\partial \eta(y; v)}{\partial y} = \mathbb{E}[|x - \eta(y; v)|^2|y]. \quad (69)$$

Thus, the posterior variance is expressed as

$$\mathbb{E}[|x - \hat{x}_{\text{MMSE}}|^2|y] = r^2 \left(1 - \left(\frac{I_1(|\zeta|)}{I_0(|\zeta|)}\right)^2\right). \quad (70)$$

APPENDIX B DERIVATION OF THE MODIFIED BESSEL FUNCTION

For completeness, we derive the analytical form of the modified Bessel function $I_n(\kappa)$. Starting from the expansion of the exponential term, we obtain

$$\int_0^{2\pi} e^{jn\psi} e^{\kappa \cos \psi} d\psi = \sum_{m=0}^{\infty} \frac{\kappa^m}{m!} \int_0^{2\pi} e^{jn\psi} \cos^m \psi d\psi. \quad (71)$$

Using Euler's formula, $\cos^m \psi$ can be expressed as a sum of complex exponentials:

$$\cos^m \psi = \frac{1}{2^m} (e^{j\psi} + e^{-j\psi})^m = \frac{1}{2^m} \sum_{k=0}^m \binom{m}{k} e^{j(2k-m)\psi}. \quad (72)$$

Substituting this into the integral yields

$$\int_0^{2\pi} e^{jn\psi} \cos^m \psi d\psi = \frac{1}{2^m} \sum_{k=0}^m \binom{m}{k} \int_0^{2\pi} e^{j(n+2k-m)\psi} d\psi. \quad (73)$$

The integral

$$\int_0^{2\pi} e^{jq\psi} d\psi = \begin{cases} 2\pi & q = 0, \\ 0 & q \neq 0, \end{cases} \quad (74)$$

implies that only the terms satisfying $n+2k-m=0$ contribute to the integral. This condition can be parameterized as $m =$

$n + 2l$, and the integral is zero for all other values of m . Therefore, for $m = n + 2l$ we obtain

$$\int_0^{2\pi} e^{jn\psi} \cos^m \psi d\psi = 2\pi \cdot \frac{(n+2l)!}{2^{n+2l} \cdot l! \cdot (n+l)!}. \quad (75)$$

Substituting this result back into (71), we obtain

$$\begin{aligned} \int_0^{2\pi} e^{jn\psi} e^{\kappa \cos \psi} d\psi &= 2\pi \sum_{l=0}^{\infty} \frac{1}{l!} \cdot \frac{1}{(n+l)!} \cdot \left(\frac{\kappa}{2}\right)^{n+2l} \\ &= 2\pi \left(\frac{\kappa}{2}\right)^n \sum_{l=0}^{\infty} \frac{1}{l! \cdot (n+l)!} \left(\frac{\kappa}{2}\right)^{2l} \\ &= 2\pi I_n(\kappa). \end{aligned} \quad (76)$$

Using the standard definition, we thus arrive at the well-known series expansion.

REFERENCES

- [1] T. L. Marzetta, "Noncooperative cellular wireless with unlimited numbers of base station antennas," *IEEE Trans. Wireless Commun.*, vol. 9, no. 11, pp. 3590–3600, 2010.
- [2] E. G. Larsson, O. Edfors, F. Tufvesson, and T. L. Marzetta, "Massive MIMO for next generation wireless systems," *IEEE Commun. Mag.*, vol. 52, no. 2, pp. 186–195, 2014.
- [3] A. Bourdoux, B. Come, and N. Khaled, "Non-reciprocal transceivers in OFDMA/SDMA systems: Impact and mitigation," in *Proc. IEEE Radio Wireless Conf. (RAWCON)*, Boston, MA, USA, 2003.
- [4] E. Björnson, J. Hoydis, M. Kountouris, and M. Debbah, "Massive MIMO systems with non-ideal hardware: Energy efficiency, estimation, and capacity limits," *IEEE Trans. Inf. Theory*, 2014.
- [5] F. Kaltenberger, D. Gesbert, and R. Knopp, "Relative channel reciprocity calibration in MIMO/TDD systems," in *Proc. Future Netw. Mobile Summit*, Florence, Italy, Jun. 2010.
- [6] J. Vieira, F. Rusek, O. Edfors, S. Malkowsky, L. Liu, and F. Tufvesson, "Reciprocity calibration for massive MIMO: Proposal, modeling, and validation," *IEEE Trans. Wireless Commun.*, 2017.
- [7] X. Jiang, A. Decurninge, K. Gopala, F. Kaltenberger, M. Guillaud, and D. Slock, "A framework for over-the-air reciprocity calibration for TDD massive MIMO systems," *IEEE Trans. Wireless Commun.*, pp. 5975–5990, Sept. 2018.
- [8] H. Q. Ngo, A. Ashikhmin, H. Yang, E. G. Larsson, and T. L. Marzetta, "Cell-free massive MIMO versus small cells," *IEEE Trans. Wireless Commun.*, vol. 16, no. 3, pp. 1834–1850, 2017.
- [9] E. Björnson and L. Sanguinetti, "Making cell-free massive MIMO competitive with MMSE processing and centralized implementation," *IEEE Trans. Wireless Commun.*, vol. 19, no. 1, pp. 77–90, 2020.
- [10] A. Papazafeiropoulos, P. Kourtessis, M. D. Renzo, S. Chatzinotas, and J. M. Senior, "Performance analysis of cell-free massive MIMO systems: A stochastic geometry approach," *IEEE Trans. Veh. Technology*, vol. 69, no. 4, pp. 3523–3537, 2020.
- [11] H. Iimori, T. Takahashi, K. Ishibashi, G. T. F. de Abreu, and W. Yu, "Grant-free access via bilinear inference for cell-free MIMO with low-coherence pilots," *IEEE Trans. Wireless Commun.*, vol. 20, no. 11, pp. 7694–7710, Nov. 2021.
- [12] T. Takahashi, H. Iimori, K. Ando, K. Ishibashi, S. Ibi, and G. T. F. de Abreu, "Bayesian receiver design via bilinear inference for cell-free massive MIMO with low-resolution ADCs," *IEEE Trans. Wireless Commun.*, vol. 22, no. 7, pp. 4756–4772, 2023.
- [13] H. A. Ammar, R. Adve, S. Shahbazpanahi, G. Boudreau, and K. V. Srinivas, "User-centric cell-free massive MIMO networks: A survey of opportunities, challenges and solutions," *IEEE Commun. Surv. Tutor.*, vol. 24, no. 1, pp. 611–652, 2022.
- [14] S. Willhammar, H. Iimori, J. Vieira, L. Sundström, F. Tufvesson, and E. G. Larsson, "Achieving distributed MIMO performance with repeater-assisted cellular massive MIMO," *IEEE Commun. Mag.*, vol. 63, no. 3, pp. 114–119, Mar. 2025.
- [15] T.-H. Vu, N. H. Tu, and V. N. Q. Bao, "Study on reconfigurable repeater-based RSMA systems," *IEEE Wireless Commun. Lett.*, vol. 14, no. 5, pp. 1371–1375, May 2025.
- [16] P. Jopanya and D. P. M. Osorio, "Enabling drone detection with swarm repeater-assisted MIMO ISAC," *arXiv preprint arXiv:2509.19119*, Sept. 2025. [Online]. Available: <https://arxiv.org/abs/2509.19119>
- [17] H. Iimori, E. Kurihara, T. Yoshida, J. Vieira, and S. Malomsoky, "Amplification strategy in repeater-assisted MIMO systems via minorization maximization," in *Proc. IEEE Global Communications Conf. (GLOBECOM)*, Kuala Lumpur, Malaysia, Dec. 2023.
- [18] M. Andersson, A. Chowdhury, and E. G. Larsson, "Is repeater-assisted massive MIMO compatible with dynamic TDD?" *arXiv preprint arXiv:2510.20998*, Jan. 2026. [Online]. Available: <https://arxiv.org/abs/2510.20998>
- [19] O. A. Topal, O. T. Demir, E. Björnson, and C. Cavdar, "Fair and energy-efficient activation control mechanisms for repeater-assisted massive MIMO," *arXiv preprint arXiv:2504.03428*, Apr. 2025. [Online]. Available: <https://arxiv.org/abs/2504.03428>
- [20] A. Chowdhury and E. G. Larsson, "On the performance of dual-antenna repeater assisted bi-static MIMO ISAC," *arXiv preprint arXiv:2511.17980*, Jan. 2026. [Online]. Available: <https://arxiv.org/abs/2511.17980>
- [21] J. Bai, A. Chowdhury, A. Hansson, and E. G. Larsson, "Repeater swarm-assisted cellular systems: Interaction stability and performance analysis," *IEEE Trans. Wireless Commun.*, vol. 25, pp. 10018–10034, Jan. 2026.
- [22] A.-T. Le, T.-H. Vu, N. H. Tu, T. N. Nguyen, L.-T. Tu, and M. Voznak, "Active-reconfigurable-repeater-assisted NOMA networks in internet of things: Reliability, security, and covertness," *IEEE Internet Things J.*, vol. 12, no. 7, pp. 8759–8772, Apr. 2025.
- [23] E. G. Larsson and J. Bai, "Stability analysis of interacting wireless repeaters," in *Proc. IEEE Int. Workshop Signal Process. Adv. Wireless Commun. (SPAWC)*, Lucca, Italy, Sept. 2024.
- [24] F. I. G. Carvalho, R. V. de O. Paiva, T. F. Maciel, V. F. Monteiro, F. R. M. Lima, D. C. Moreira, D. A. Sousa, B. Makki, M. Åström, and L. Bao, "Network-controlled repeater – An introduction," *IEEE Commun. Stand. Mag.*, Aug. 2025, early Access.
- [25] R. Nie, L. Chen, N. Zhao, Y. Chen, F. R. Yu, and G. Wei, "Relaying systems with reciprocity mismatch: Impact analysis and calibration," *IEEE Trans. Commun.*, vol. 68, no. 7, pp. 4035–4049, 2020.
- [26] Y. Ma, D. Zhu, B. Li, and P. Liang, "Channel estimation error and beamforming performance in repeater-enhanced massive MIMO systems," in *Proc. IEEE 26th Annu. Int. Symp. Pers., Indoor, Mobile Radio Commun. (PIMRC)*, Hong Kong, China, Aug. 2015.
- [27] E. G. Larsson, J. Vieira, and P. Frenger, "Reciprocity calibration of dual-antenna repeaters," *IEEE Wireless Commun. Lett.*, vol. 13, no. 6, pp. 1606–1610, 2024.
- [28] K. Ito, T. Takahashi, S. Ibi, and S. Sampei, "Bayesian joint channel and data estimation for correlated large MIMO with non-orthogonal pilots," in *Proc. IEEE Int. Conf. Commun. (ICC)*, Montreal, Canada, June 2021.
- [29] T. Takahashi, H. Iimori, K. Ishibashi, S. Ibi, and G. T. F. de Abreu, "Bayesian bilinear inference for joint channel tracking and data detection in millimeter-wave MIMO systems," *IEEE Trans. Wireless Commun.*, vol. 23, no. 9, pp. 11136–11153, 2024.
- [30] K. R. R. Ranasinghe, H. Seok Rou, G. Thadeu Freitas de Abreu, T. Takahashi, and K. Ito, "Joint channel, data, and radar parameter estimation for AFDM systems in doubly-dispersive channels," *IEEE Trans. Wireless Commun.*, vol. 24, no. 2, pp. 1602–1619, 2025.
- [31] U. Gustavsson, C. Sánchez-Perez, T. Eriksson, F. Athley, G. Durisi, P. Landin, K. Hausmair, C. Fager, and L. Svensson, "On the impact of hardware impairments on massive MIMO," in *Proc. IEEE Glob. Commun. Conf. Workshops (GLOBECOM WS)*, 2014.
- [32] F. Athley, G. Durisi, and U. Gustavsson, "Analysis of massive MIMO with hardware impairments and different channel models," in *Proc. Eur. Conf. Antennas Propag. (EuCAP)*, Lisbon, Portugal, 2015.
- [33] K. Ito, T. Takahashi, S. Ibi, and S. Sampei, "Bilinear gaussian belief propagation for massive MIMO detection with non-orthogonal pilots," *IEEE Trans. Commun.*, vol. 72, no. 2, pp. 1045–1061, 2024.
- [34] H. Iimori, T. Takahashi, K. Ishibashi, G. T. F. de Abreu, D. González G., and O. Gonsa, "Joint activity and channel estimation for extra-large MIMO systems," *IEEE Trans. Wireless Commun.*, vol. 21, no. 9, pp. 7253–7270, 2022.
- [35] A. Chockalingam and B. S. Rajan, *Large MIMO Systems*. Cambridge University Press, 2014.
- [36] J. Vieira, F. Rusek, and F. Tufvesson, "Reciprocity calibration methods for massive MIMO based on antenna coupling," in *Proc. IEEE Glob. Commun. Conf. (GLOBECOM)*, Austin, USA, Dec. 2014.